Mon. Not. R. Astron. Soc. **000**, 000–000 (0000) Printed 5 October 2018 (MN LaTeX style file v2.2)

Quantifying the evidence for the current speed-up of the Universe with low and intermediate-redshift data. A more model-independent approach

Adrià Gómez-Valent*
Departament de Física Quàntica i Astrofísica, and Institute of Cosmos Sciences, Universitat de Barcelona, Av. Diagonal 647 E-08028 Barcelona, Catalonia

5 October 2018

ABSTRACT
We reconstruct in this paper the deceleration and jerk parameters as functions of the cosmological redshift from data on cosmic chronometers (CCH), baryon acoustic oscillations (BAOs), and the Pantheon+MCT compilation of supernovae of Type Ia (SnIa). The reconstruction is carried out with the Weighted Function Regression method, previously introduced by Gómez-Valent & Amendola (2018). It improves the usual cosmographic approach by automatically implementing Occam's razor criterion. This makes our procedure to be more free of model and parametrization dependencies than many other analyses in the literature. The reconstructed functions are fully compatible with the predictions for the concordance model. In addition, we also discuss the confidence level at which we can claim that the Universe (assumed to be flat, homogeneous and isotropic) is currently accelerating. According to Jeffreys' scale and jargon, we find moderate evidence in favor of such speed-up using the data on SnIa+CCH, and very strong one when we also use data on BAOs. The measured current value of the deceleration parameter in the latter case reads $q_0 \sim -0.60 \pm 0.10$, and for the deceleration-acceleration transition redshift we find $z_t \sim 0.8 \pm 0.10$. The former is $\sim 6\sigma$ away from 0. This is in stark contrast, for instance, with the $\sim 17\sigma$ that are found in the context of the flat ΛCDM even without including the BAOs data. This indicates that cosmography and Occam's razor criterion play a crucial role in this discussion, and that estimating the evidence for positive acceleration only in the framework of a particular cosmological model or parametrization is clearly insufficient.

Key words: cosmological parameters – dark energy – cosmology:observations.

1 INTRODUCTION

Is the Universe currently undergoing a positive acceleration phase? Certainly, we can only reply this question within the margins of accuracy set by the cosmological observations, i.e. the most that we can do is to answer yes or no with the confidence level permitted by the data at our disposal. Thus, it would be better to reformulate the question in an alternative way: what is the evidence in favor of the current speed-up of the Universe according to the existing cosmological data? This work is mainly focused on answering this pivotal question using low and intermediate-redshift data, trying to do it from a very skeptical perspective and removing from the analysis as much as possible the model-dependencies that could eventually bias our final answer. These model-dependencies are actually plaguing many other works in the literature, which address the problem either in the framework of concrete cosmological models, using particular parametrizations of the deceleration parameter or the jerk (cf. formulas (1) and (7), respectively, and Sect. 3.1), or even truncated cosmographical series describing the luminosity distance or the Hubble function in which the highest order of the expansion is fixed to a concrete value (see the list of references below). None of these analyses are model-independent in a strict sense, and therefore neither the derived confidence regions for the current value of the deceleration parameter, which describes the acceleration status of the Universe at present. It turns out that the evidence that is obtained in favor of a positive-accelerated Universe depends very strongly on the model or parametrization that is assumed in the analysis (we will show this explicitly in Sect. 3.2), so the evidence for positive acceleration that is obtained from the data can only carry an absolute and hence powerful statistical meaning when it is inferred in a full-fledged

* adriagova@fqa.ub.edu

model-independent way. Otherwise, it only tells us what is the evidence in the concrete model or parametrization employed in that particular study, and thus we are not in a position to answer our question in a completely secure manner. This work aims to alleviate this situation and pave the way to the obtention of a more model-independent determination of the cosmographical functions, but before entering the details of our reconstruction method let us review some of the studies on these issues and corresponding results that one can find in the literature on the subject, which is quite vast.

The first important hints of positive acceleration were reported in the late nineties by the High-Z Supernova Search Team (Riess et al. 1998) and the Supernova Cosmology Project (Perlmutter et al. 1999) collaborations, from the first measurements of the apparent magnitude of supernovae of Type Ia (SnIa) at high redshifts. The samples contained individuals up to $z = 0.97$ and 0.83, respectively, and also included low-redshift SnIa of $z \lesssim 0.15$ from the Calán/Tololo Supernova Survey and, in the first case, from the CfA sample too. In the context of the non-flat ΛCDM model they found the probability for the presence of a positive cosmological constant (Λ) in Einstein's field equations to be $P(\Lambda > 0) = 99\%$, and restricting the analysis to the purely flat ΛCDM, i.e. setting the current spatial curvature density $\Omega_k^{(0)} = 0$, they found $\sim 3\sigma$ evidence in favor of the current positive acceleration of the Universe. Subsequent studies incorporated the data of even higher-redshift SnIa discovered with the Hubble Space Telescope (HST) (Riess et al. 2001; Turner & Riess 2002; Knop et al. 2003; Riess et al. 2004), at $z \gtrsim 1$. This allowed to also find compelling evidence for a deceleration-acceleration transition at $z_t \sim 0.5$. For instance, in (Riess et al. 2004) the authors made use of a parametrization for the deceleration parameter of the form $q(z) = q_0 + q_1 z$, with $q_0 = q(0)$ and $q_1 = \frac{dq}{dz}$. The deceleration parameter is directly related to the second derivative of the scale factor with respect to the cosmic time t (Sandage 1970; Weinberg 1972),

$$q = -\frac{\ddot{a}}{aH^2}\,, \tag{1}$$

with $H = \dot{a}/a$ being the Hubble function and the dot denoting such derivative. Considering a flat Universe they obtained $P(q_0 < 0) = 99.2\%$ and $P(q_1 > 0) = 99.8\%$, and thus important evidence in favor of the current positive acceleration of the Cosmos and the existence of a deceleration-acceleration transition point in the past, more concretely at $z_t = 0.46 \pm 0.13$, with $q(z_t) = 0$.

These pioneering studies made possible the first accurate estimations of the deceleration parameter of the history. Therein the authors explored two of the routes that have been later on subsequently revisited by the cosmological community once and again to infer the evidence for a negative q_0 and the existence of a transition redshift, using different data sources. In e.g. (Riess et al. 1998; Perlmutter et al. 1999; Knop et al. 2003) the authors assumed concrete cosmological models, mainly the flat and non-flat ΛCDM, and derived according to the data available at the time and in that particular cosmological scenarios the confidence intervals for q_0. This approach makes direct use of the gravitational field equations in a particular theoretical setting, where all the sources of the energy-momentum tensor and/or the deviations from standard General Relativity (GR) are specified beforehand. Conversely, Turner & Riess (2002) and Riess et al. (2004) directly parametrized the deceleration parameter without focusing in any concrete cosmological model and hence tried to orient their analyses in a more "cosmographical" way, although of course such parametrizations are not free of model-dependencies by definition, as we will explicitly show in this paper.

Using cosmography (also dubbed cosmokinetics or Friedmannless Cosmology) one can extract kinematic information about the Universe from measurements of cosmological distances by only assuming the Cosmological Principle, which is clearly fulfilled at very large (cosmological) scales. Cosmic microwave background (CMB) observations and the inflationary paradigm also allow us to consider a flat Universe, which helps to break important degeneracies in the cosmographical framework, e.g. between the jerk and $\Omega_k^{(0)}$ (Visser 2004, 2005; Dunsby & Luongo 2016). In this geometrical approach one does not need to introduce any assumption on the metric theory of gravity or the matter-energy content of the Universe, which is something very positive. Cosmography was boosted thanks to the papers by Visser (2004, 2005), in which he extended the cosmographical formalism of previous works (see e.g. those by Sandage (1970) and Weinberg (1972)) to include also higher order terms in the expansion of the cosmological distances, as the jerk and the snap (which we will discuss in detail later on). Although the cosmographical methodology cannot shed much light on the ultimate cause of the positive acceleration of the Universe, some parameters as the jerk can be employed as direct tests of the ΛCDM and the potential time-variation of the dark energy (DE) density, see e.g. (Sahni et al. 2003; Blandford et al. 2005). Moreover, it can certainly help us to answer important questions related to its kinematic properties without relying on a particular cosmological model, but this statement should be actually duly qualified. Cosmographical expansions of cosmological distances are still parametrizations. They are truncated Taylor series developed around e.g. $z = 0$. Choosing the concrete order at which the series is cut can be tricky and the derived constraints for the various parameters involved in the expansion can be highly dependent on this choice, as was already noted by Elgarøy & Multamäki (2006). We can of course proceed applying some model-selection criteria based on: the computation of exact Bayesian evidence, see e.g. (Amendola & Tsujikawa 2015; Amendola 2018); the Akaike or Bayesian criteria (Akaike 1974; Schwarz 1978); or even make use of the reduced chi-squared statistic. Nevertheless, regardless of how we select the "right" order of the cosmographical expansion according to the existing data the following questions should be still settled down: how should we proceed if two nested cosmographical expansions behaved very similarly in terms of model selection criteria. Should we choose the one with e.g. closest reduced chi-squared statistic to 1, and throw the other one away? Would we be legitimated to do this, independently of how close the two expansions behaved in practice? Wouldn't we be loosing precious statistical information then? We firmly believe that the usual cosmographical method must be improved in order to deal with all these subtle points, and try to remove the remaining degree of subjectivity that is inherent to the choice of the highest order of the cosmographical expansion. We will do this through the so-called Weighted Function Regression (WFR) method, which was already introduced in (Gómez-Valent & Amendola 2018)[1] to reconstruct the Hubble function using data on $H(z_i)$ at different redshifts extracted from cosmic chronometers (CCH) with the differential-age technique, together with the data from the SnIa of the Pantheon compilation and the HST CANDELS and CLASH Multy-Cycle Treasury (MCT) programs. In this paper we will make use of the same data sources to study the two next-to-leading order terms in the expansion of the scale factor, i.e. the deceleration and jerk parameters. We will also study the impact of some intermediate-redshift data obtained from the analysis of baryon acoustic oscillations (BAOs). The WFR method implements in practice the Occam razor criterion, not by selecting only one cosmographical expansion among the various (nested) alternatives, but incorporating all of them consistently in our calculations using appropriate and rigorous Bayesian tools. This allows us to reconstruct the aforesaid cosmographical functions in a fairer and more model and parametrization-independent way. We hope to improve thereby the methodology applied and the constraints reported on e.g., q_0 or z_t, in many other works in the literature, as those based on concrete parametrizations of the deceleration or the jerk parameters (Turner & Riess 2002; Riess et al. 2004; Elgarøy & Multamäki 2006; Shapiro & Turner 2006; Rapetti et al. 2007; Gong & Wang 2007; Ishida et al. 2008; Cunha & Lima 2008; Guimarães 2009; Mörtsell & Clarkson 2009; Xu, Li & Lu 2009; Cunha 2009; Lu, Xu & Liu 2011; Guimarães & Lima 2011; Giostri et al. 2012; Nair, Jhingan & Jain 2012; Zhai et al. 2013; Akarsu et al. 2014; Mukherjee & Banerjee 2016; Vargas dos Santos, Reis & Waga 2016; Mamon & Das 2017; Jesus, Holanda & Pereira 2018; Mamon & Bamba 2018), truncated cosmographical series (Cattoën & Visser 2007a,b; Xu, Li & Lu 2009; Vitagliano et al. 2010; Luongo 2011; Xu & Wang 2011; Rubin & Hayden 2016; Jesus, Holanda & Pereira 2018; Dutta et al. 2018; Heneka 2018), alternative expansions of the luminosity distance (Semiz & Çamlibel 2015), or specific cosmological models, including also various parametrizations of the DE density or the DE equation of state (EoS) parameter, see e.g. (Riess et al. 1998; Perlmutter et al. 1999; Riess et al. 2001; Turner & Riess 2002; Knop et al. 2003; Riess et al. 2004; Rapetti et al. 2007; Nielsen, Guffanti & Sarkar 2016; Rubin & Hayden 2016; Ringermacher & Mead 2016; Haridasu et al. 2017; Mamon 2018). Other authors have also applied alternative techniques to reconstruct the expansion history of the Universe in a model-independent way and derive constraints on the deceleration parameter, e.g. using the smoothing method of (Shafieloo et al. 2006; Shafieloo 2007, 2012), principal component analyses (Shapiro & Turner 2006; Mörtsell & Clarkson 2009), Gaussian processes (Haridasu et al. 2018), or piecewise natural cubic splines (Tutusaus, Lamine & Blanchard 2018). These methods are interesting and useful, but also have their own drawbacks. We deem that the WFR method rises as a good alternative to put objective and fair constraints to the most relevant kinematic functions, by using low and intermediate-redshift data.

This paper is organized as follows. In Sect. 2 we describe in detail the data sets that we employ in the reconstruction of the deceleration and jerk parameters. In Sect. 3 we motivate and explain the WFR method after introducing some basic elements of cosmography that we need in order to apply this reconstruction technique. In Sect. 4 we present and discuss our results, including the plots with the main reconstructed cosmographical functions and some tables. We finally present our conclusions in Sect. 5.

2 THE DATA SETS

In this section we list the data that we employ in our reconstruction of the various cosmographical functions we are interested in with the weighted function regression method. We also provide the corresponding references, discuss the model dependencies and assumptions behind these data, and the way they are introduced in our analysis in order to: (i) mitigate as much as possible the effect of some of these model-dependencies; (ii) incorporate unaccounted systematic uncertainties that were not taken into account in the original references; and (iii) ease the computation of evidences and the practical implementation of the WFR method. As mentioned already at the title and abstract levels, we make use of only low and intermediate-redshift data, i.e. at $z \lesssim 2.5$. The reason is double. On the one hand, the data on CCH and SnIa are cosmology-independent, and the data on $H(z_i)$ extracted from the radial component of anisotropic BAOs can be dealt with also in a way such that the model-dependencies can be strongly suppressed, as we will explain in Sect. 2.2. On the other hand, the cosmographic approach works optimally only with data at this approximate redshift range. It is difficult to include in the analysis e.g. the CMB data, since the latter would force us to consider higher order terms in the cosmographical expansions, which would probably reduce the constraining power on the lowest-order cosmographical parameters, as e.g. q_0. This is easy to understand if we think of cosmography as what it indeed consists on, i.e. Taylor expansions of the scale factor and derived quantities around the current time. Moreover, the redshift range of these data points already covers the fraction of the cosmological history we are mainly interested in, including the deceleration-acceleration transition point.

2.1 Data on $E(z)$ from the Pantheon+MCT SnIa compilation

In this work we use the Hubble rate data points, i.e. $E(z_i) = H(z_i)/H_0$ with $H_0 = H(z = 0)$, provided in (Riess et al. 2018b) for six different redshifts in the range $z \in [0.07, 1.5]$. They compress very effectively the information about the 1048 SnIa at $z < 1.5$ that take part of the Pantheon compilation (Scolnic et al. 2018) (which includes the 740 SnIa of the joint light-curve analysis sample compiled by Betoule et al. (2014)), and the 15 SnIa at $z > 1$ of the CANDELS and CLASH Multy-Cycle Treasury programs obtained by the HST, 9 of which are at $1.5 < z < 2.3$. Riess et al. (2018b)

[1] In (Gómez-Valent & Amendola 2018) we called this method Weighted *Polynomial* Regression instead of Weighted *Function* Regression, just because in that paper we used polynomials for the basis functions. In this work, though, we will also use non-polynomial expressions (see Sect. 3.1), so this change in the name is needed.

z_i	$E(z_i)$	Correlation matrix					
0.07	0.997 ± 0.023	1.00					
0.20	1.111 ± 0.020	0.39	1.00				
0.35	1.128 ± 0.037	0.53	-0.14	1.00			
0.55	1.364 ± 0.063	0.37	0.37	-0.16	1.00		
0.90	1.52 ± 0.12	0.01	-0.08	0.17	-0.39	1.00	
1.50	2.78 ± 0.59	-0.03	-0.07	-0.07	0.13	-0.16	1.00

Table 1. Data on the Hubble rate $E(z_i)$ and corresponding correlation matrix from the Pantheon+MCT SnIa compilation (Scolnic et al. 2018; Riess et al. 2018b). The correlation matrix is of course symmetric, so we only write the elements of its lower triangle. See the text for details.

converted the raw SnIa measurements into data on $E(z)$ by parametrizing $E^{-1}(z)$ at those six redshifts z_i. The integral over E^{-1} that defines the luminosity distance is then obtained by interpolating between z_i with cubic Hermite polynomials. Finally, the overall constant H_0 is marginalized away along with the absolute supernovae magnitude, see (Riess et al. 2018b) for further details. The corresponding values of $E^{-1}(z_i)$ are Gaussian in very good approximation and are shown in Table 6 of (Riess et al. 2018b), together with the corresponding correlation matrix. We present their inverse, $E(z_i)$, and the correlation matrix in Table 1 for completeness and because we will use the $E(z)$-data in the reconstruction of the Hubble rate. This will allow us to compute the weights of the WFR method exactly in this case. Notice that the correlation matrix for the $E(z)$-data is very similar to the one that contains the correlations between the $E^{-1}(z_i)$-values. The firsts five points are almost perfectly Gaussian too. In contrast, $E(z = 1.5)$ is not normal-distributed at such good level, see the last plot in Fig. 1. The best-fit value reads $E(1.5) = 2.67^{+0.83}_{-0.52}$. Nevertheless, we have opted to fit a Gaussian to the exact histogram as a first approximation, obtaining $E(1.5) = 2.78 \pm 0.59$[2]. This works quite well, since as we already showed in (Gómez-Valent & Amendola 2018), the relative uncertainty of $E(z = 1.5)$ is considerably larger than the other five data points and hence its impact on the final shape of the reconstructed functions is much lower. In addition, it is easier and more practical to deal with a multivariate Gaussian distribution, rather than considering the small departures from it, especially when their impact is so small, as in the case under study. As we will see in Sect. 3, this is because in this way we can derive analytically also the constraints on the coefficients of the reconstructed Hubble rate, which are also Gaussian-distributed due to the fact that the latter is built linear in the parameters. This allows us to save valuable computational time.

It is important to remark that these values on $E(z_i)$ have been obtained by assuming a flat Universe and the Cosmological Principle, and thus are model-dependent in this sense, cf. (Riess et al. 2018b). The homogeneity and isotropy of the Universe at large scales are features exceedingly sustained by radiation backgrounds as CMB observations, and counts of sources observed at wavelengths ranging from radio to gamma rays. We know moreover that the flatness assumption is quite reasonable if our main aim is to use these data points to reconstruct $E(z)$ around the current time. Note e.g. that the TT+lowP+lensing+BAO analysis carried out by the Planck Collaboration VI (2018) leads to a value of $\Omega_k^{(0)} = 0.0007 \pm 0.0019$ at 1σ c.l., which is fully compatible with the flat Universe scenario; or the analysis by Ooba, Ratra & Sugiyama (2018), which in this case favors a closed Universe, although the central value for $\Omega_k^{(0)}$ is still low, around -0.006 when the model is confronted to the TT,TE,EE+lowP+lensing+BAO data. One can easily check that the relative change on $H(z)$ caused by these tiny deviations from flatness is really small, being around 0.3% in the redshift range $0 \leq z \leq 2$. This is of course much smaller than the relative uncertainties of our data points and also than the one of the reconstructed functions (see e.g. Figs. 2-3). Thus, given the sensitivity of the data we are dealing with, the assumption of a flat Universe has a derisory impact on our results. Moreover, it also allows us to break the existing strong degeneracy between the current values of the jerk and the snap parameters and $\Omega_k^{(0)}$ (Visser 2004, 2005; Dunsby & Luongo 2016), and this is of course crucial to obtain tighter constraints on these cosmographical quantities.

We also want to mention that the Hubble rate data of Table 1 have been obtained without considering the potential time evolution of the SnIa intrinsic luminosity, hence sticking to the standard approach in the literature. Tutusaus et al. (2017) interestingly showed that when this assumption is not taken for granted a decelerated low-redshift power law model of the type $a(t) \sim t^n$ (with $n < 1$) is able to fit the low-redshift background data as well as, or even slightly better, than the ΛCDM. Riess et al. (2018b) argued, though, that when SnIa data at $z > 1.5$ are included in the analysis the ΛCDM is ~ 60 times more probable than a marginally accelerating power-law cosmology with $n = 1.04$. They conclude that there is no motivation for including the potential redshift-dependence of the intrinsic SnIa luminosity based on astrophysical or empirical considerations.

2.2 Data on $E(z)$ from cosmic chronometers and BAOs

Spectroscopic dating techniques of passivelyevolving galaxies, i.e. galaxies with old stellar populations and low star formation rates, have become a good tool to obtain observational values of the Hubble function at redshifts $z \lesssim 2$ (see the work by Jimenez & Loeb (2002) and also the references in Table 2). The measurements of CCH listed in Table 2 have been obtained from galaxies located at different angles in the sky. Under the coverage of the Cosmological Principle the dependence of the CCH data on the angle and location of the measured galaxies is removed, and therefore the H's be-

[2] Other authors, as Haridasu et al. (2018) and Pinho, Casas & Amendola (2018) just symmetrize the upper and lower bounds of $E(1.5)$ provided in (Riess et al. 2018b), without adapting its central value. This yields $E(1.5) = 2.67 \pm 0.68$. No important differences in the final results are obtained when this value is used instead of ours due to the reasons exposed above in the text.

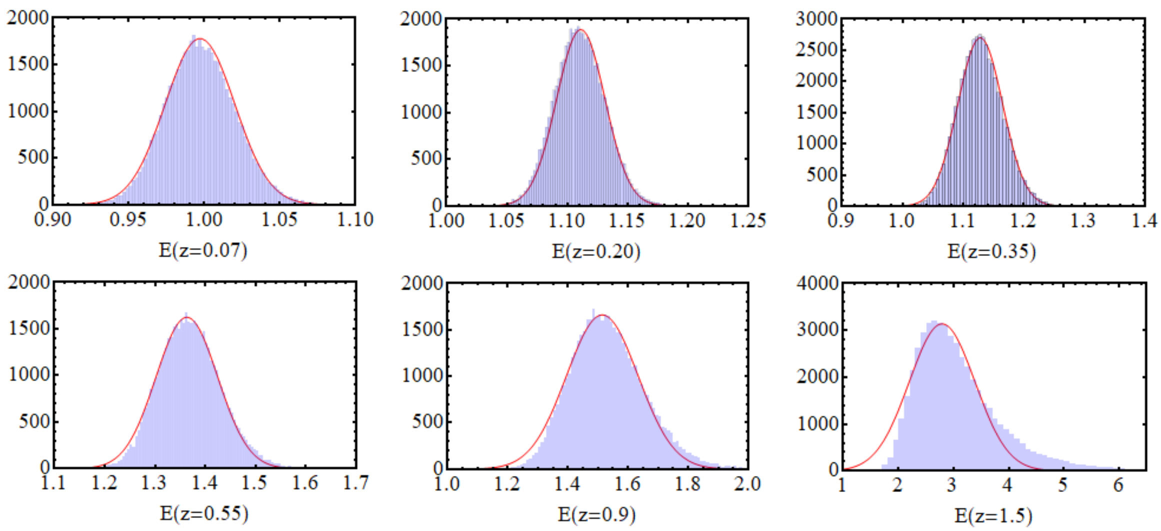

Figure 1. Histograms for the six values of $E(z_i)$ derived from the Pantheon+MCT SnIa compilation. They have been obtained, together with the corresponding covariance matrix, by inverting the values of $E^{-1}(z_i)$ provided in (Riess et al. 2018b) with a Monte Carlo routine (Metropolis et al. 1953; Hastings 1970), with which we have generated a Markov chain of $5 \cdot 10^4$ points. We also superimpose the fitted Gaussians (in red) in order to show that the exact distributions are normal in very good approximation for the first five redshifts, and in lesser extent for the sixth one. See the comments in the main text of Sect. 2.1.

come just functions of the redshift. These measurements are independent of the Cepheid distance scale and do not rely on any particular cosmological model, although are subject to other sources of systematic uncertainties, as to the ones associated to the modeling of stellar ages, see e.g. (Moresco et al. 2012; Moresco et al. 2016), which is carried out through the so-called stellar population synthesis techniques (SPS), and also to a possible contamination due to the presence of young stellar components in such quiescent galaxies (López-Corredoira & Vazdekis 2017; López-Corredoira et al. 2018; Moresco et al. 2018). Given a pair of ensembles of passively-evolving galaxies at two different redshifts it is possible to infer dz/dt from observations under the assumption of a concrete SPS model and compute $H(z) = -(1+z)^{-1}dz/dt$. Thus, cosmic chronometers allow us to directly obtain the value of the Hubble function at different redshifts, contrary to other probes which do not directly measure $H(z)$, but integrated quantities as e.g. luminosity distances. In Table 2 we list the CCH data points used in our analyses, including their corresponding uncertainties σ_i. We point out that we have used a diagonal covariance matrix for these data, i.e. $C_{ij} = \sigma_i^2\delta_{ij}$. Moreover, we have not directly used in this study the original data points provided in the references of Table 2, $H^{\rm ori}(z_i)$'s, but the corresponding processed values, $H^{\rm pro}(z_i)$'s, obtained upon correcting the former in order to include the systematic effects mentioned before. Namely, for the data of references (Moresco et al. 2012; Moresco et al. 2016), where the values of $H^{\rm ori}(z_i)$ obtained from the two alternative SPS models of (Bruzual & Charlot 2003) and (Maraston & Strömbäck 2011) are provided (from now on we will refer to them as BC03 and MaStro, respectively), we have opted to compute the corresponding processed value at each redshift by computing the weighted sum of the two,

$$H^{\rm pro}(z_i) = \frac{\sum_{j=1}^{2} \frac{H_j^{\rm ori}(z_i)}{\sigma_j^2(z_i)}}{\sum_{j=1}^{2} \sigma_j^{-2}(z_i)} \,. \qquad (2)$$

The $\sigma_j(z_i)$'s do not refer to the uncertainties of the second column of Table 2, but to the corrected ones,

$$\sigma_j(z_i) = \sqrt{\tilde{\sigma}_j^2(z_i) + |H_1^{\rm ori}(z_i) - H_2^{\rm ori}(z_i)|^2 + [0.025H_j^{\rm ori}(z_i)]^2} \,, \qquad (3)$$

where $\tilde{\sigma}_j(z_i)$ for $j = 1, 2$ are just the original uncertainties (which *do* refer to those of the second column of Table 2), the second term in the square root is introduced to account for the systematic error that is due to the choice of the SPS model, and the last term accounts for the potential contamination of the passively-evolving galaxies for the presence of a young stellar component. Moresco et al. (2018) reanalyzed the data presented in (Moresco et al. 2012; Moresco et al. 2016) to assess the impact of this effect and showed that the young population contamination is actually minimal and consistent with zero given the current uncertainties. They calculated that at most it would bias the determinations on $H(z_i)$ by $0.4-1\%$ (at 1σ, $0.8-2.3\%$ at 2σ), well below the current errors. We have been conservative, though, and added a 2.5% systematic uncertainty (at 1σ) not only to the values reported in (Moresco et al. 2012; Moresco et al. 2016), but also to those provided in the other references, see the Table 2. We have assumed, therefore, that the conclusions of (Moresco et al. 2018) can also be extended to the rest of studies from which we have compiled the CCH data. The results of the processed $H^{\rm pro}(z_i)$'s, which incorporate the corrections of formulas (2) and (3), are listed in the third column of the same table. The uncertainties of the

z_i	$H^{\rm ori}(z_i)$ [$\mathrm{km\,s^{-1}Mpc^{-1}}$]	$H^{\rm pro}(z_i)$ [$\mathrm{km\,s^{-1}Mpc^{-1}}$]	References
0.07	69.0 ± 19.6	69.0 ± 19.7	Zhang et al. (2014)
0.09	69.0 ± 12.0	69.0 ± 12.1	Jiménez et al. (2003)
0.12	68.6 ± 26.2	68.6 ± 26.3	Zhang et al. (2014)
0.17	83.0 ± 8.0	83.0 ± 8.3	Simon, Verde & Jiménez (2005)
0.1791	75.0 ± 4.0 81.0 ± 5.0	77.8 ± 8.1	Moresco et al. (2012)
0.1993	75.0 ± 5.0 81.0 ± 6.0	77.7 ± 8.7	Moresco et al. (2012)
0.2	72.9 ± 29.6	72.9 ± 29.7	Zhang et al. (2014)
0.27	77.0 ± 14.0	77.0 ± 14.1	Simon, Verde & Jiménez (2005)
0.28	88.8 ± 36.6	88.8 ± 36.7	Zhang et al. (2014)
0.3519	83.0 ± 14.0 88.0 ± 16.0	85.2 ± 16.9	Moresco et al. (2012)
0.3802	83.0 ± 13.5 89.3 ± 14.1	86.0 ± 15.6	Moresco et al. (2016)
0.4	95.0 ± 17.0	95.0 ± 17.2	Simon, Verde & Jiménez (2005)
0.4004	77.0 ± 10.2 82.8 ± 10.6	79.8 ± 12.3	Moresco et al. (2016)
0.4247	87.1 ± 11.2 93.7 ± 11.7	90.3 ± 13.6	Moresco et al. (2016)
0.4497	92.8 ± 12.9 99.7 ± 13.4	96.1 ± 15.3	Moresco et al. (2016)
0.47	89.0 ± 49.6	89.0 ± 49.6	Ratsimbazafy et al. (2017)
0.4783	80.9 ± 9.0 86.6 ± 8.7	83.8 ± 10.8	Moresco et al. (2016)
0.48	97.0 ± 62.0	97.0 ± 62.0	Stern et al. (2010)
0.5929	104.0 ± 13.0 110.0 ± 15.0	106.7 ± 16.4	Moresco et al. (2012)
0.6797	92.0 ± 8.0 98.0 ± 10.0	94.6 ± 11.9	Moresco et al. (2012)
0.7812	105.0 ± 12.0 88.0 ± 11.0	96.3 ± 21.0	Moresco et al. (2012)
0.8754	125.0 ± 17.0 124.0 ± 17.0	124.5 ± 17.3	Moresco et al. (2012)
0.88	90.0 ± 40.0	90.0 ± 40.1	Stern et al. (2010)
0.9	117.0 ± 23.0	117.0 ± 23.2	Simon, Verde & Jiménez (2005)
1.037	154.0 ± 20.0 113.0 ± 15.0	132.5 ± 45.8	Moresco et al. (2012)
1.3	168.0 ± 17.0	168.0 ± 17.5	Simon, Verde & Jiménez (2005)
1.363	160.0 ± 33.6	160.0 ± 33.8	Moresco (2015)
1.43	177.0 ± 18.0	177.0 ± 18.5	Simon, Verde & Jiménez (2005)
1.53	140.0 ± 14.0	140.0 ± 14.4	Simon, Verde & Jiménez (2005)
1.75	202.0 ± 40.0	202.0 ± 40.3	Simon, Verde & Jiménez (2005)
1.965	186.5 ± 50.4	186.5 ± 50.6	Moresco (2015)

Table 2. Data on $H(z_i)$ obtained from CCH. See the quoted references and the text for details. Notice that we write both, the original values provided in these references ($H^{\rm ori}$) and also the processed ones ($H^{\rm pro}$), i.e. those that are obtained upon the implementation of the corrections explained in Sect. 2.2. In the case of references (Moresco et al. 2012; Moresco et al. 2016) the authors provide the values obtained with the BC03 and MaStro SPS models. We list both here, being those at the top of the corresponding row (second column) the BC03 ones and those at the bottom the MaStro ones.

$H^{\rm pro}(z_i)$'s from (Moresco et al. 2012; Moresco et al. 2016) are taken to be the greatest of the two σ_j's in each case. For the rest of references they are given by the corresponding $\sigma(z_i)$'s.

In this work we also include data on BAOs. More concretely, we consider the radial component of the anisotropic BAOs obtained from the measurement of: (i) the power spectrum and bispectrum from the Baryon Oscillation Spectroscopic Survey (BOSS) data release 12 galaxies (Gil-Marín et al. 2017), $H(z=0.32)r_s(z_d)=(11.55\pm0.38)\cdot10^3\,\mathrm{km\,s^{-1}}$ and $H(z=0.57)r_s(z_d)=(14.02\pm0.22)\cdot10^3\,\mathrm{km\,s^{-1}}$; (ii) the complete Sloan Digital Sky Survey (SDSS) III Lyα-quasar auto and cross-correlation functions (Mas des Bourboux et al. 2017), $c/[H(z=2.40)r_s(z_d)]=8.94\pm0.22$; and (iii) the SDSS-IV extended BOSS data release 14 quasar sample (Gil-Marín et al. 2018), $H(z=1.52)r_s(z_d)=(24.0\pm1.8)\cdot10^3\,\mathrm{km\,s^{-1}}$. The theoretical expression of the sound horizon at the redshift of the radiation drag z_d reads,

$$r_s(z_d)=\int_{z_d}^{\infty}\frac{c_s(z)}{H(z)}dz\,, \tag{4}$$

where $c_s(z)$ is the sound speed in the baryon-photon plasma. $r_s(z_d)$ obviously depends on the physics at very high redshifts, i.e. at $z>z_d\sim\mathcal{O}(10^3)$, and, in particular, on the Hubble function at those epochs. This complicates in principle the cosmographic analysis, since the latter is only consistent and effective when only data at low and intermediate redshifts are included. One way to deal with this problem is to apply a reasonable (as model-independent as possible) prior for $r_s(z_d)$ in order to re-express the BAOs constraints just in terms of the value of the Hubble function at the intermediate redshifts explored by the various surveys. The Planck Collaboration VI (2018) has found $r_s(z_d)=(147.21\pm0.48)$ Mpc fitting the ΛCDM model to the TT+lowE CMB data, almost exactly the same value that reported two years before in (Planck Collaboration XIII 2016) using the TT+lowP data set, $r_s(z_d)=(147.33\pm0.49)$ Mpc. Verde et al. (2017) showed, though, that when non-standard dark radiation components are allowed to be present in the pre-recombination epoch a slightly larger value of $r_s(z_d)$ is preferred, with substantial larger relative uncertainty, $r_s(z_d)=(150\pm5)$ Mpc. We deem this is a more model-independent estimation of the sound horizon at the drag epoch, which covers the Planck preferred value and range at $< 1\sigma$. This is the value we are going to use as a prior in our study to transform the BAOs information into direct constraints on $H(z_i)$. But we are actually not only interested in doing this, but also in obtaining direct constraints on the Hubble rate $E(z_i)$ from the aforesaid data on BAOs and also the CCH data points listed in Table 2. It is highly convenient to work only with data on $E(z_i)$ because, as we will see later on more in detail, the combination of data on $H(z_i)$ and $E(z_i)$ would make appear in the description of $H(z)$ some non-linearities due to the product of H_0 with the parameters of the linear expansion that we will use for the reconstruction of $E(z)$. These non-linearities would pose a problem because then the parameters of $E(z)$ would not be Gaussian-distributed, and the exact computation of the evidences would have to be carried out numerically, which would imply a much more expensive budget in terms of computational time. In contrast, if we only use data on $E(z_i)$ we are able to compute the exact evidences and Bayes ratios (and thus the weights of the WFR method, see Sect. 3.4) in a pure analytical way, just because the data is Gaussian-distributed and $E(z)$ will be constructed linear in the parameters. We will provide the corresponding expressions in the subsequent section. Hence, according to these explanations it becomes clear that we need to also include a prior on H_0 (again, as model-independent as possible) in our analysis. The choice of this prior is not a straightforward task. It is very well-known that there exists a 3.5σ tension between the local determination of H_0 by Riess et al. (2018a), $H_0 = (73.48 \pm 1.66)$ km s^{-1}Mpc^{-1}, and the one found by the Planck Collaboration VI (2018) assuming the ΛCDM and using e.g. the TT+lowE CMB data, $H_0 = (66.88 \pm 0.92)$ km s^{-1}Mpc^{-1}. If this tension is caused by some kind of systematic error affecting the data or due to the need of new physics beyond the standard model is still unknown. Other works that make use of the cosmic distance ladder find very similar results to the one reported by Riess et al. (2018a), see e.g. (Cardona, Kunz & Pettorino 2017; Jang & Lee 2017; Zhang et al. 2017; Follin & Knox 2018), and are also consistent with preceding studies, as e.g. (Riess et al. 2011; Riess et al. 2016). Any important systematic error has been neither found in Planck's determination. Addison et al. (2018) showed that independent analyses from Planck using alternative high-redshift data also lead to results in non-negligible tension with the local value of H_0. For instance, using the constraints on the primordial abundance of deuterium and galaxy and Lyα forest BAOs data they found $H_0 = (66.98 \pm 1.18)$ km s^{-1}Mpc^{-1} in the context of the ΛCDM. Assuming the same model, Bonvin et al. (2017) found $H_0 = (71.9^{+2.4}_{-3.0})$ km s^{-1}Mpc^{-1} by analyzing the gravitational time delay of the light rays coming from the three multiply imaged quasar system HE 0435 − 1223, and Birrer et al. (2018) $H_0 = (68.8^{+5.4}_{-5.1})$ km s^{-1}Mpc^{-1} from the doubly imaged quasar SDSS 1206+4332. In these cases there is no tension with the local determination. Recently, it has also been possible to measure the Hubble parameter using the gravitational wave signal of the neutron star merger GW17081716 and its electromagnetic counterpart (Abbott et al. 2017; Guidorzi et al. 2017), providing high values of H_0, but still with very large uncertainties (70^{+12}_{-8} and $75.5^{+11.6}_{-9.6}$ km s^{-1}Mpc^{-1}, respectively). They are completely independent from the underlying cosmology and the cosmic distance ladder. The claimed reduction of the degeneracy between the source distance and the weakly constrained viewing angle has allowed to considerably reduce also the uncertainty of H_0, yielding $68.9^{+4.7}_{-4.6}$ km s^{-1}Mpc^{-1} (Hotokezaka et al. 2018). The central value is now more compatible with the local determinations, although some criticisms to this new estimation have been also drawn (Dado & Dar 2018). It is also worth to mention the cosmology-independent analyses carried out in (Yu, Ratra & Wang 2018; Gómez-Valent & Amendola 2018; Feeney et al. 2018; Haridasu et al. 2018; Lemos et al. 2018), where use is made of different combinations of cosmological low and intermediate-redshift data involving SnIa, CCH and BAOs. A value of $H_0 \sim 68.5$ km s^{-1}Mpc^{-1} is obtained, see these references for details. Some other authors, as Marra et al. (2013) and, more recently, Camarena & Marra (2018), have studied the impact of the cosmic variance on the local determination of H_0, and conclude that although it can certainly play a role its effect is unable to explain the whole discrepancy between the HST and Planck's values. Romano (2018) explains in his paper that the use by Riess et al. of the 2M++ density field map (which covers redshifts $z \leq 0.06$) to compute peculiar velocity flows could be biasing their results, since there is evidence of the existence of local radial inhomogeneities extending in different directions up to a redshift of about 0.07 (Keenan, Barger & Cowie 2013), and according to Romano (2018) the 40% of the Cepheids used by Riess et al. (2018a) would be affected. In view of the large dispersion of values of H_0 found in the vast literature, we opt to adopt in this work the following prior in our main analyses: $H_0 = (70 \pm 5)$ km s^{-1}Mpc^{-1}, which basically covers the values of interest without relying exclusively on the low or the high parameter region. We have also studied, though, the impact of the (less conservative) priors provided in (Riess et al. 2018a) and (Planck Collaboration VI 2018) and checked that they lead to fully compatible results for the shape of the cosmographical functions and, in particular, for the value and the uncertainty of q_0. Finally, we consider a correlation coefficient $\rho = -0.56$ between H_0 and $r_s(z_d)$ in the Gaussian prior of the main analyses, inspired by the ΛCDM Planck's constraints. We have also explored other values around -0.6. The results are kept consistent too. Using this two-dimensional prior we can convert the CCH values of $H(z_i)$ and the BAOs data into direct constraints on $E(z_i)$, which can later on be employed together with the SnIa data listed in Table 1 to perform the cosmographical analysis with the WFR method, using only data on the Hubble rate at different redshifts. We have checked that the distribution of the processed CCH and BAOs data on $E(z_i)$ is very well approximated by a multivariate Gaussian, which is crucial to compute analytically the evidence associated to the various cosmographical expansions of $E(z)$, see Sect. 3.4. As expected, although the original CCH and BAOs data are uncorrelated, some correlations appear between the corresponding transformed values of $E(z_i)$ due to the use of the prior on H_0 and $r_s(z_d)$. We have taken all these correlations into account.

3 THE WEIGHTED FUNCTION REGRESSION METHOD

3.1 Cosmography through $E(z)$: deceleration, jerk, and snap parameters

Assuming (as we do in this paper) that the Universe is flat, homogeneous and isotropic, the square of the space-time element interval can be written in the usual Friedmann-Lemaître-Robertson-Walker (FLRW) form,

$$ds^2 = dt^2 - a^2(t)d\vec{x}^2\,, \tag{5}$$

with $a(t)$ being the scale factor and x_i with $i = 1,2,3$ the comoving space coordinates. The former can be Taylor-expanded around the current time t_0,

$$a(t) = 1 + \sum_{n=1}^{\infty} \frac{1}{n!}\frac{d^n a}{dt^n}\Big|_{t=t_0}(t-t_0)^n\,, \tag{6}$$

where we have set $a(t_0) = 1$. It can also be written in terms of the current values of the various cosmographical functions. Up to the fourth order in t, the expansion involves the Hubble and deceleration parameters (see Eq. (1) and below), as well as the jerk and the snap, which read respectively (Visser 2004, 2005),

$$j = \frac{1}{aH^3}\frac{d^3a}{dt^3}\,, \qquad s = \frac{1}{aH^4}\frac{d^4a}{dt^4}\,. \tag{7}$$

Upon substitution in (6) one obtains,

$$a(t) = 1 + H_0(t-t_0) - \frac{1}{2}q_0H_0^2(t-t_0)^2 + \frac{1}{6}j_0H_0^3(t-t_0)^3 + \frac{1}{24}s_0H_0^4(t-t_0)^4 + ...\,, \tag{8}$$

[3] with the subscript 0 referring to present-day quantities. As we have shown in Sect. 2, we will deal with data on the Hubble rate in order to extract the cosmographical information. Thus, it is better to directly express it in the cosmographical form (instead of working with the expansion of the scale factor), and as a function of the redshift (instead of the cosmic time), since the former is the physical variable with which we make contact with observations. The Taylor series of $H(z)$ around $z = 0$ is just given by

$$H(z) = H_0 + \sum_{n=1}^{\infty} \frac{1}{n!}\frac{d^n H}{dz^n}\Big|_{z=0} z^n\,. \tag{9}$$

In order to write this expansion in terms of the cosmographical parameters we firstly need to express the cosmographical functions (1) and (7) in terms of the derivatives of $H(z)$ with respect to the redshift z. Making use of $d/dt = -(1+z)H(z)d/dz$ and after a little bit of algebra we obtain the following relations,

$$q(z) = -1 + \frac{1+z}{H(z)}\frac{dH}{dz}\,, \tag{10}$$

$$j(z) = q^2(z) + \frac{(1+z)^2}{H(z)}\frac{d^2H}{dz^2}\,, \tag{11}$$

$$s(z) = 3[q^2(z) + q^3(z) - j(z)] - 4q(z)j(z) - \frac{(1+z)^3}{H(z)}\frac{d^3H}{dz^3}\,. \tag{12}$$

We can isolate the derivatives of the Hubble function from these expressions and use them in (9). Dividing the result by H_0 one finally obtains the expansion of the Hubble rate in terms of the current values of the cosmographical functions, as desired,

$$E(z) = 1 + (1+q_0)z + \frac{1}{2}(j_0 - q_0^2)z^2 + \frac{1}{6}(3q_0^3 + 3q_0^2 - 3j_0 - 4q_0j_0 - s_0)z^3 + ... \tag{13}$$

As it was already reported by Cattoën & Visser (2007a,b) this Taylor series (which is built in z, around $z = 0$) has radius of convergence $\Delta z = 1$ and therefore we cannot expect it to describe the correct physical behavior at redshifts larger than one. One possible way to solve this problem is to apply a shift in the pivoting redshift in order to increase the radius of convergence. Another viable solution consists on using the variable $y = 1 - a = z/(1+z)$ instead of directly z, as it is also suggested in (Cattoën & Visser 2007a,b), see therein for further details. The Taylor series of the Hubble rate around $y = 0$ reads as follows,

$$E(y) = 1 + \sum_{n=1}^{\infty} \frac{1}{n!}\frac{d^n E}{dy^n}\Big|_{y=0} y^n\,,$$

and can be also written as

$$E(z) = 1 + (1+q_0)\frac{z}{1+z} + (j_0 - q_0^2 + 2 + 2q_0)\frac{z^2}{2(1+z)^2} + (6 + 6q_0 - 3q_0^2 + 3q_0^3 + 3j_0 - 4j_0q_0 - s_0)\frac{z^3}{6(1+z)^3} + ... \tag{14}$$

As mentioned before, (14) is *a priori* more appropriate than (13) because the former solves the formal convergence problem discussed above, but we remark that this convergence problem arises when we deal with the full series (13) and not when we use truncated expressions derived from it. One can check that Taylor-expanding $(1+z)^{-1} = 1 - z + z^2 - z^3 + \mathcal{O}(z^4)$ in all the terms of the last expression one retrieves (13), so both formulas are consistent. Notice that we can use in principle some truncated forms of (13) and (14) to extract important kinematic information about the Cosmos' expansion without making any assumption about the matter-energy sources of the gravitational field equations nor the gravitational theory itself, i.e. without assuming anything about the ultimate cause of the Universe's dynamics. We cannot only extract the values of q_0, j_0 and s_0, but we can also reconstruct $q(z)$, $j(z)$ and $s(z)$ using (10)-(12). These truncated series are, though, not free from problems, as we will duly explain in the next subsection. We will mitigate these problems in the context of the WFR method (see Sect. 3.3 for details). In Sect. 4 we will show that the reconstructed shapes of $E(z)$ obtained using (13) and (14) and the WFR method are fully consistent. Converseley, the situation for $q(z)$ is different. Although the central values derived with

[3] The minus sign of the third term on the right-hand side of (8) is due to the definition of the deceleration parameter (1). The latter is still defined as in (Sandage 1970), when it was thought that the Universe was currently decelerating, i.e. $\ddot{a}(t_0) < 0$, due to the dominance of the non-relativistic matter. The minus sign of (1) made q_0 to be positive. After the works by Riess et al. (1998) and Perlmutter et al. (1999) there is probably no *raison d'être* for this minus sign, but nevertheless it has been preserved in the definition, as originally.

(13) and (14) are compatible, the corresponding uncertainties change quite a lot depending on the parametrization employed in the analysis. We will explain why in Sect. 4.

In this work we will also apply the WFR method using expansions of $q(z)$ instead of expansions of the Hubble rate. More concretely, we will explore the following two possibilities,

$$q(z) = q_0 + q_1 z + q_2 z^2 + ... \tag{15}$$

and

$$q(z) = q_0 + \frac{q_1 z}{1+z} + \frac{q_2 z^2}{(1+z)^2} + ... \tag{16}$$

to reconstruct the deceleration parameter. We will show that we find consistent reconstructed shapes for $q(z)$. One can also rewrite (11) in terms of only $q(z)$,

$$j(z) = 2q^2(z) + q(z) + (1+z)\frac{dq}{dz} \,. \tag{17}$$

This formula eases the direct reconstruction of the jerk from (15) and (16).

In Sect. 4 we provide all the details about the various reconstructions we have carried out in this work, and provide the constraints for q_0 and j_0 derived from them.

3.2 Estimation of q_0 in some model and parametrization-dependent scenarios, and the need of an improved cosmographical approach

We dedicate this section to motivate the need of improving those works in the literature that obtain constraints on the cosmographical functions in the framework of concrete cosmological models, using particular parametrizations of the cosmographical functions, or even truncated cosmographical series in which the maximum order of the expansion is chosen in an *ad hoc* way in more or lesser extent. All these approaches are perfectly licit, of course, but one cannot claim to extract model-independent information about the Universe's kinematics from them. As an example, we will explicitly derive the constraints for q_0 that are obtained in some of these scenarios just to show that both, the central values and, more conspicuously, their corresponding uncertainties, are very sensitive to the particular framework chosen to carry out the analysis. This means that the results and conclusions derived from these studies can be in some cases partially or completely biased. Thus, we are forced to search for an alternative approach that proves capable of reducing the existing degree of subjectivity. Section 3.3 will be devoted to the description of one of such methods, the WFR.

We start now analyzing some cosmological models in standard GR, considering the Cosmological Principle and a flat Universe. In this framework it is possible to write the deceleration parameter in terms of the energy densities and pressures of the various species that fill the Universe by using (10) together with the Friedmann and energy conservation equations,

$$q(z) = -1 + \frac{3}{2}\frac{\sum\limits_i [\rho_i(z) + p_i(z)]}{\sum\limits_i \rho_i(z)} \,, \tag{18}$$

where the subscript i labels all the matter-energy components. Let us focus now in the late-time expansion, when the radiation energy density is negligible versus the non-relativistic matter one. If the latter and the DE are self-conserved then

$$\rho_m(z) = \rho_m^{(0)}(1+z)^3 \quad ; \quad \rho_D(z) = \rho_D^{(0)} e^{3\int_0^z \frac{1+w(\tilde{z})}{1+\tilde{z}} d\tilde{z}} \,. \tag{19}$$

The evolution of the DE density is thus specified by the DE EoS parameter $w(z) = p_D(z)/\rho_D(z)$, and *vice versa*. As the pressure of the matter component is negligible versus its energy density, one can write the deceleration parameter in the case under study only in terms of $w(z)$ by plugging (19) into (18). There is thus a one-to-one correspondence between $q(z)$ and the EoS parameter of the self-conserved DE. We analyze here three models: (i) the ΛCDM, in which $w(z) = -1$ and the DE density remains constant throughout all the cosmic expansion, see e.g. (Amendola & Tsujikawa 2015) and references therein; (ii) the XCDM (also known as wCDM) parametrization of the DE EoS parameter (Turner & White 1997), in which $w(z) = w_0$, with w_0 being a constant that can in principle acquire both, quintessence ($w_0 > -1$) or phantom-like ($w_0 < -1$) values; and (iii) the CPL parametrization (Chevallier & Polarski 2001; Linder 2003, 2004), the next-to-leading order correction of the XCDM, in which $w(z) = w_0 + w_1 z/(1+z)$. The EoS parameter has in the latter case some evolution and could (at least, in principle) pass through the phantom divide. We choose these models basically because of their simplicity and also because they have a different number of free parameters. The XCDM and CPL have one and two more parameters than the concordance model, respectively. In the CPL parametrization the square of the Hubble rate reads,

$$E^2(z) = \Omega_m^{(0)}(1+z)^3 + (1-\Omega_m^{(0)})e^{-\frac{3w_1 z}{(1+z)}}(1+z)^{3(1+w_0+w_1)} \,, \tag{20}$$

with $\Omega_m^{(0)} = \rho_m^{(0)}/(\rho_m^{(0)} + \rho_D^{(0)})$ being the matter density parameter. For the ΛCDM and the XCDM the corresponding expressions are obtained straightforwardly, by just setting in (20) $(w_0, w_1) = (-1, 0)$ in the first case, and $w_1 = 0$ in the second one. Using these formulas we can confront the three models to the Pantheon+MCT and the CCH data (cf. Tables 1 and 2, respectively, and the comments in Sect. 2). The results are listed in Table 3, where we also show the value of q_0 that is obtained for each of the models under study. For the XCDM and CPL parametrizations the theoretical expression of the deceleration parameter reads,

$$q_0 = -1 + \frac{3}{2}\left[1 + w_0(1-\Omega_m^{(0)})\right] \,, \tag{21}$$

whereas for the ΛCDM we have to set $w_0 = -1$ in this formula. Notice that the values that are obtained for this kinematic quantity are compatible in the three models, and hence fully consistent (cf. the penultimate column of Table 3). Nevertheless, the uncertainties are quite different in magnitude, being in the XCDM (CPL) a factor ~ 3 (~ 6) larger than in the ΛCDM. The reason is obvious, in the XCDM (CPL) we have one (two) more free parameter(s) than in the concordance model, so the constraints that are obtained from the data for the various fitting parameters and derived quantities are weaker for the former models. But then, which is the level of evidence at which we can state that $q_0 < 0$, i.e. in favor of the current positive-accelerated phase of the Universe? In the ΛCDM the value of q_0 is $\sim 17\sigma$ away from $q_0 = 0$, in the XCDM such distance is of roughly 6σ, and

Model	$\Omega_m^{(0)}$	H_0 [km s^{-1}Mpc^{-1}]	w_0	w_1	q_0	$\chi^2_{\rm min}$
ΛCDM	0.295 ± 0.021	70.45 ± 2.36	-1	0	-0.554 ± 0.032	15.74
XCDM	0.306 ± 0.051	70.31 ± 2.42	-1.03 ± 0.15	0	-0.578 ± 0.099	15.74
CPL	0.301 ± 0.104	70.34 ± 2.47	-1.04 ± 0.16	0.10 ± 1.78	-0.494 ± 0.195	15.74

Table 3. Fitting results obtained for the ΛCDM model and the XCDM and CPL parametrizations of the DE EoS, by using the Pantheon+MCT SnIa and the CCH data described in Sect. 2. The derived deceleration parameter q_0 and the minimum value of the χ^2-function for each model are also provided.

in the CPL it is "only" of $\sim 2.5\sigma$, so the differences are not precisely small. The minimum values of the χ^2-function obtained in the ΛCDM, XCDM and CPL (cf. again Table 3, last column), tell us that these models are able to fit equally well the data, so we have to use some method to penalize the use of extra parameters and see which is the most favored scenario. Whatever it is the method employed we will find e.g. that the ΛCDM is preferred over the XCDM and CPL. Although the values of $\chi^2_{\rm min}$ are the same for the three models, there is a penalization for the XCDM and CPL with respect to the ΛCDM which is caused by the addition of the free parameters w_0 and (w_0, w_1), respectively. But still, up to what extent can we rely on the uncertainty of q_0 that is obtained in the framework of the ΛCDM? Are all these constraints representative of the underlying "true" model describing the Cosmos? It could well be not the case, since even if the ΛCDM is more preferred than the XCDM and CPL, we have made some important assumptions that might have a non-negligible impact on our results and, more conspicuously, on the corresponding uncertainties. Apart from assuming the isotropy, homogeneity and flatness of the Universe, we have assumed that the correct theory of gravity is Einstein's GR together with the self-conservation of matter and DE, and the presence of a cosmological constant triggering the cosmic acceleration. Some of these can be considered very strong assumptions and, certainly, dispensing with them would lead us to more loose constraints on q_0 than those obtained in the context of the ΛCDM. Thus, in order to extract more objective constraints on q_0 we should definitely abandon the model-dependent approach.

Cosmography can help us to extract model-independent constraints on the various kinematic quantities when the data employed are themselves free of model-dependencies, which unfortunately is not always the case. We have to remark, though, one important point which is usually overlooked in many works in the literature. Although the cosmographical functions (e.g. $q(z)$ or $j(z)$) can be obtained in a very model-independent way, they are *not* model-independent *per se*. For instance, by just building and fitting parametrized expressions of these cosmographical functions to the data we are not led to fully model-independent results. Given a parametrized form of $q(z)$ one can integrate (10) to obtain the associated Hubble function, and use it to compute the rest of higher order cosmographical functions as well, as the jerk (11) and the snap (12). It is also possible to relate the aforementioned parametrization of $q(z)$ with various models of DE in the standard GR scenario. Once we have $H(z)$ we can obtain the DE pressure $p_D(z)$ using the equation,

$$3H^2(z) - 2(1+z)H(z)\frac{dH}{dz} = -8\pi G p_D(z)\,. \qquad (22)$$

Notice that the concrete form of the density $\rho_D(z)$ is not unequivocally determined and will exclusively depend on the way we split the conservation equation for the DE and matter,

$$-(1+z)\sum_i \frac{d\rho_i}{dz} + 3\sum_i [\rho_i(z) + p_i(z)] = 0\,, \qquad (23)$$

i.e. on the specific form of the source function $Q(z)$ that describes the transfer of energy from one sector to the other,

$$-(1+z)\frac{d\rho_m}{dz} + 3\rho_m(z) = Q(z)\,,$$

$$-(1+z)\frac{d\rho_D}{dz} + 3[\rho_D(z) + p_D(z)] = -Q(z)\,. \qquad (24)$$

In order to show this in more concrete terms, let us put a simple example in which we assume that $q(z) = q_0$, with q_0 being a constant. Upon integration of (10) we obtain,

$$H(z) = H_0(1+z)^{1+q_0}\,, \qquad (25)$$

and using this result in (22) we compute the DE pressure,

$$p_D(z) = -\frac{3H_0^2}{8\pi G}(1+z)^{2(1+q_0)}\left[1 - \frac{2}{3}(1+q_0)\right]. \qquad (26)$$

If we assume that matter and DE are self-conserved, i.e. that $Q(z) = 0$, we are led to the following expression for the DE density,

$$\rho_D(z) = \frac{3H_0^2}{8\pi G}(1+z)^{2(1+q_0)} - \rho_m^{(0)}(1+z)^3\,, \qquad (27)$$

and the standard matter dilution law $\rho_m(z) = \rho_m^{(0)}(1+z)^3$. Different expressions for the energy densities are obtained when $Q(z) \neq 0$, and they change with the particular form of $Q(z)$. The same happens for more elaborated parametrizations of the deceleration parameter, showing in all cases that we can associate an infinite set of DE models to a given parametrization of $q(z)$. This seems to point out that the problem is somehow alleviated with respect to the cases analyzed before in which particular cosmological models were assumed, since now we can obtain constraints on cosmographical functions which are not only valid for a concrete model, but are also extensible to a whole family of them. In this sense, this approach is more model-independent. Despite this, such constraints are still very reliant on the particular parametrization chosen, as can be explicitly checked in Table 4, where we show the fitting results for four alternative parametrizations of $q(z)$. Again, the level of evidence in favor of the current positive acceleration of the Universe varies a lot depending on the particular choice of $q(z)$. It ranges from the $\sim 3\sigma$ significance of the most complex model (the one in the fourth row) to the $\sim 8\sigma$ found using e.g. $q(z) = q_0$, and the latter is in strong tension with the values obtained with the other parametrizations. This situation was already noticed by Elgarøy & Multamäki (2006), who applied model selection criteria in order to select the most favored parametrization of $q(z)$ among those that they

$q(z)$-parametrization	H_0 [km s^{-1}Mpc^{-1}]	q_0	q_1	q_2	$\chi^2_{\rm min}$
q_0	72.29 ± 2.37	-0.288 ± 0.036	–	–	32.64
$q_0 + q_1 z$	70.35 ± 2.47	-0.503 ± 0.063	0.66 ± 0.16	–	16.26
$q_0 + q_1 z/(1+z)$	70.55 ± 2.46	-0.611 ± 0.084	1.50 ± 0.36	–	15.74
$q_0 + q_1 z/(1+z) + q_2 z^2/(1+z)^2$	70.49 ± 2.51	-0.59 ± 0.20	1.33 ± 1.89	0.31 ± 3.24	15.74

Table 4. As in Table 3, but for four alternative parametrizations of $q(z)$.

studied in their paper. This is definitely better than just choosing one parametrization in a fully blind way, but nevertheless we deem that this does not completely solve the problem, since there can be several parametrizations leading to different associated values of e.g. q_0 that in terms of model selection criteria offer a similar efficiency. Picking just one form of $q(z)$ might therefore lead us still to biased conclusions and to underestimate the uncertainties of the measured quantities, even if we use model-selection criteria to carry out our choice. Thus, depending on the physical question we are interested to answer we are still forced to search for an alternative approach which does not depend on particular parametrizations of $q(z)$ or any other alternative cosmographical function. In the next section we describe the WFR method, a generalization of the procedure applied in (Elgarøy & Multamäki 2006) which is able to mitigate even more the problem, and to go one step further concerning the model-independence of these kind of analyses.

3.3 Reconstruction of $E(z)$ with the WFR method

Those works in which the authors choose a particular truncated cosmographical series to carry out the fitting analysis are also susceptible to the problems that we have exposed in the preceding subsection. In this case the situation is not very different from choosing a concrete parametrization of $q(z)$. To understand why, let us focus on the cosmographical expansions (13) and (14). If we cut these series at a given order and apply (10) we can obtain the form of $q(z)$ associated to the aforesaid truncated series of $E(z)$. The problem we encounter is therefore completely analogous to the one described in the last part of Sect. 3.2. Now we will try to alleviate it in the cosmographical context of (13) and (14). The mathematical structure of these expansions of the Hubble rate have something in common: they are built linear in the coefficients c_i,

$$E(z) = 1 + \sum_{i=1}^{\infty} c_i g_i(z)\,, \tag{28}$$

where the c_i's are constants that can be expressed in terms of the cosmographical parameters, i.e. q_0, j_0, s_0, etc.[4], and the $g_i(z)$'s are functions of the redshift with a very simple structure, $g_i(z) = [g_1(z)]^i$, being $g_1(z) = z$ in (13) and $g_1(z) = z/(1+z)$ in (14). They are usually referred to as *basis* functions. Instead of relying on one particular truncated series,

$$E_J(z) = 1 + \sum_{i=1}^{J} c_i g_i(z)\,, \tag{29}$$

and thus set J to a concrete value in our study, we opt to incorporate the information about all the nested expansions (obtained by changing J) in order to skip the problem of choosing just one among them in the fitting analysis. Let us call M_1, M_2,..., M_N the cosmographical expansions of order $J = 1, 2,..., N$, respectively, with N being the number of data points used in the analysis. That is, let us conceive each expansion as a different model, and compute the probability density associated to the fact of having a certain shape for the Hubble rate as follows,

$$P[E(z)] = k\cdot[P(E(z)|M_1)P(M_1)+...+P(E(z)|M_N)P(M_N)]\,, \tag{30}$$

where k is just a normalization constant that must be fixed by imposing

$$\int [\mathcal{D}E]\, P[E(z)] = 1\,. \tag{31}$$

Taking into account that

$$\int [\mathcal{D}E]\, P(E(z)|M_J) = 1 \quad \forall J \in [1, N] \tag{32}$$

and

$$\sum_{J=1}^{N} P(M_J) = 1\,, \tag{33}$$

we find $k = 1$ and therefore:

$$P[E(z)] = \sum_{J=1}^{N} P(E(z)|M_J)P(M_J)\,. \tag{34}$$

We now denote M_* as the most probable model and rewrite the last expression as follows,

$$P[E(z)] = P(M_*) \sum_{J=1}^{N} P(E(z)|M_J)\frac{P(M_J)}{P(M_*)}\,, \tag{35}$$

where $\frac{P(M_J)}{P(M_*)}$ can be identified with the Bayes ratio B_{J*}, i.e. the ratio of evidences

$$B_{J*} = \frac{\mathcal{E}_J}{\mathcal{E}_*} = \frac{\int \mathcal{L}(\mathcal{D}|\vec{c}_J)\pi(\vec{c}_J)d\vec{c}_J}{\int \mathcal{L}(\mathcal{D}|\vec{c}_*)\pi(\vec{c}_*)d\vec{c}_*}\,, \tag{36}$$

with $\mathcal{L}(\mathcal{D}|\vec{c}_J)$ being the likelihood function, which is a function of the coefficients entering the model J, $\vec{c}_J$, and the data set $\mathcal{D}$ (which of course is common for all the models), and $\pi(\vec{c}_J)$ being the prior, see e.g. (Amendola & Tsujikawa 2015; Amendola 2018). M_* is formally defined as the model with largest evidence in the whole set $\{M_J\}$. Using (33) one finds

$$P(M_*) = \left(\sum_{J=1}^{N} B_{J*}\right)^{-1}\,, \tag{37}$$

[4] For the sake of clarity, we remark that we will refer to the c_i's as coefficients of the expansion, and to the q_0, j_0, s_0, etc. as the cosmographical parameters.

so (35) can be finally written as

$$P[E(z)] = \frac{\sum_{J=1}^{N} P(E(z)|M_J)B_{J*}}{\sum_{J=1}^{N} B_{J*}} \,. \tag{38}$$

This is the central expression of the weighted function regression method, where the weights are directly given by the Bayes factors. Notice that from (38) we can compute the (weighted) moments and related quantities too. For instance, the weighted mean and variance read,

$$\bar{E}(z) = \frac{\sum_{J=1}^{N} \bar{E}_J(z)B_{J*}}{\sum_{J=1}^{N} B_{J*}} \,, \tag{39}$$

$$\sigma^2(z) = \frac{\sum_{J=1}^{N} [\sigma_J^2(z) + (\bar{E}_J(z))^2]B_{J*}}{\sum_{J=1}^{N} B_{J*}} - (\bar{E}(z))^2 \,, \tag{40}$$

where $\bar{E}_J(z)$ and $\sigma_J(z)$ are the mean and standard deviation computed in the model J (we will show in Sect. 3.4 how to calculate them analytically in the case under study). We remark here that these functions will differ in general from the best-fit function and its associated 68.3% c.l. bands due to the possible deviations from Gaussianity encountered in the final reconstructions. It is also possible to estimate the effective number of parameters in the final reconstruction, using

$$N_{\rm eff} = \frac{\sum_{J=1}^{N} JB_{J*}}{\sum_{J=1}^{N} B_{J*}} \,. \tag{41}$$

The machinery explained in this subsection was already employed in (Gómez-Valent& Amendola 2018) to reconstruct the Hubble function in the light of the CCH and Pantheon+MCT SnIa data, using (39) and (40), and evaluating the Bayes ratio approximately with the help of the Akaike (Akaike 1974) and Bayesian (Schwarz 1978) information criteria as explained in Sect. 4.2 of our past paper. Now we aim to reconstruct $E(z)$, $q(z)$ and $j(z)$ using the weighted function regression formalism too, but improving the methodology in two important aspects with respect to (Gómez-Valent& Amendola 2018), namely: (i) here we will compute not the mean and variance of these functions, but the best-fit and corresponding exact 1σ confidence regions; and (ii) we will calculate the exact Bayes ratios with the formula (36), instead of using approximations of it. In the case under study it is possible to compute the exact expressions for the evidences analytically because the fitting functions (29) are in all cases, i.e. $\forall J$, linear in the parameters c_i and, in addition, the data on $E(z)$ described in Sect. 2 are Gaussian-distributed in very good approximation. In the next subsection we explicitly derive the formula for the evidence, which plays a very important role in the WFR method, since it is in charge of controlling the weight of the various models in the final distribution (38).

3.4 Computation of evidences and other quantities of interest

We begin this subsection reviewing the main expressions needed for fitting Gaussian-distributed data with functions that are linear in the coefficients, as in the case that concerns us. If we have a collection $\mathcal{D} = \{(z_\mu, y_\mu),\ \mu = 1, ..., N,\ N \geq J\}$ of Gaussian-distributed data points with covariance matrix C, and we want to fit (29) to them we have to maximize the likelihood

$$\mathcal{L}(\mathcal{D}|\vec{c}) = \frac{1}{(2\pi)^{N/2}\sqrt{|C|}} e^{-\frac{1}{2}[y_\mu - E(z_\mu;\vec{a})]C^{-1}_{\mu\beta}[y_\beta - E(z_\beta;\vec{a})]} \tag{42}$$

with respect to the elements of the vector of coefficients $\vec{c}$. We have omitted here the subscripts J for simplicity, but it is important to keep in mind we are referring to a particular model M_J, so the theoretical expression for the Hubble rate is characteristic of this concrete model, and so are the covariance matrices and mean values of the coefficients that will appear in the subsequent formulas for both, the likelihood and the prior distributions. Notice also that in the last formula we are using the Einstein summation convention, as we will do in all the forthcoming expressions unless stated otherwise. We use Greek letters for indexes labeling data points, and Latin ones for those labeling the terms of $E(z)$, as in (29). Due to the linearity of the latter in the coefficients it is possible to rewrite the likelihood (42) as a multivariate Gaussian distribution for the coefficients too, i.e.

$$\mathcal{L}(\mathcal{D}|\vec{c}) = \frac{e^{-\chi^2_{\rm min}/2}}{(2\pi)^{N/2}\sqrt{|C|}} e^{-\frac{1}{2}(c_i - \bar{l}_i)F_{ij}(c_j - \bar{l}_j)} \,, \tag{43}$$

where $\chi^2_{\rm min} = \chi^2(\bar{\vec{c}})$,

$$F_{ij} = G^i_\mu C^{-1}_{\mu\beta} G^j_\beta \tag{44}$$

is the inverse covariance matrix of the coefficients, also known as Fisher matrix, $G^i_\mu \equiv g_i(z_\mu)$, and

$$\bar{l}_i = y_\mu C^{-1}_{\mu\beta} G^j_\beta F^{-1}_{ij} \tag{45}$$

is the mean value derived from the likelihood for the coefficient c_i. It is straightforward to compute the mean function $\bar{E}_J(z)$ and covariance matrix $\text{cov}[E_J(z), E_J(z')]$ associated to the model M_J. It can be done as follows (here we write again the sum symbols explicitly),

$$\bar{E}_J(z) = 1 + \sum_{i=1}^{J} \bar{l}_i g_i(z) \,, \tag{46}$$

$$\text{cov}[E_J(z), E_J(z')] = \sum_{i,j=1}^{J} F^{-1}_{ij} g_i(z) g_j(z') \,. \tag{47}$$

The variance of the reconstructed function is just $\sigma^2_J(z) = \text{cov}[E_J(z), E_J(z)]$. These expressions are involved in the computation of (39) and (40). Now, we have all the ingredients to derive the compact formula for the posterior distribution in one particular model M_J. It can also be found in many other references, as in (Nesseris & García-Bellido 2013; Amendola & Tsujikawa 2015; Amendola 2018), but we add this information here too for completeness. The product

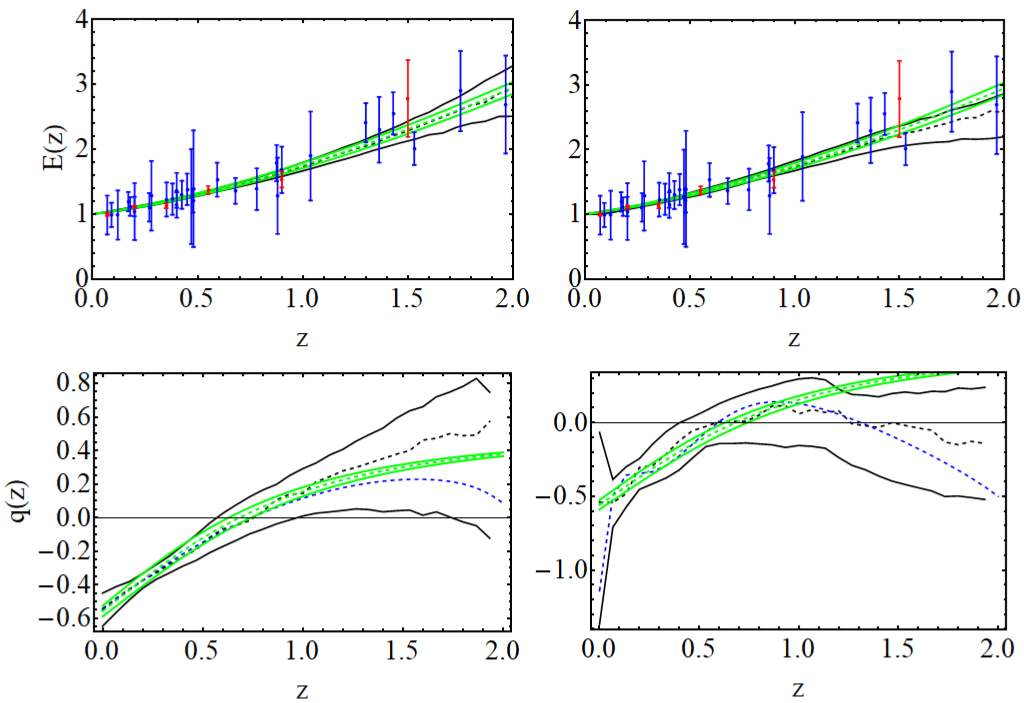

Figure 2. In black, best-fit values and 1σ uncertainties of the reconstructed functions $E(z)$ (top row) and the derived $q(z)$ (bottom row) that are obtained using the WFR method as described in Sects. 3.3 and 3.4, based on the expansions (13) (plots in the left column) and (14) (in the right one), and making use of the Pantheon+MCT (prior) and CCH (likelihood) data. These data points are incorporated to the upper plots with red and blue error bars, respectively. The blue-dashed curves in the lower plots refer to the mean of $q(z)$. We also show (in green) the central curves and 1σ-bands for the ΛCDM model, obtained using the best-fit values of Table 3. See the related comments in the main text.

of the Gaussian prior,

$$\pi(\vec{c}) = \frac{1}{(2\pi)^{J/2}\sqrt{|P|}} e^{-\frac{1}{2}(c_i-\bar{p}_i)P^{-1}_{ij}(c_j-\bar{p}_j)}\,, \tag{48}$$

with the likelihood (43) can be written as follows,

$$\mathcal{L}(\mathcal{D}|\vec{c})\pi(\vec{c}) = \tag{49}$$
$$\frac{e^{-\frac{1}{2}(\chi^2_{\rm min}+\bar{l}_i\bar{l}_jF_{ij}+\bar{p}_i\bar{p}_jP^{-1}_{ij}-\bar{d}_i\bar{d}_jD^{-1}_{ij})}}{(2\pi)^{(J+N)/2}\sqrt{|P||C|}} e^{-\frac{1}{2}(c_i-\bar{d}_i)D^{-1}_{ij}(c_j-\bar{d}_j)}\,,$$

with

$$D^{-1}_{ij} = F_{ij} + P^{-1}_{ij} \tag{50}$$

being the inverse of the posterior covariance matrix, and

$$\bar{d}_k = D_{ki}(F_{ij}\bar{l}_j + P^{-1}_{ij}\bar{p}_j) \tag{51}$$

the posterior mean of the coefficient c_k. The latter coincides with the best-fit value, since the posterior distribution is also a multivariate Gaussian. The integration of (49) with respect to the coefficients of the model, $\vec{c}$, is straightforward and leads us to the final expression for the evidence that enters the formula of the Bayes ratio (36),

$$\mathcal{E} = \frac{1}{(2\pi)^{N/2}\sqrt{|C|}}\sqrt{\frac{|D|}{|P|}}\, e^{-\frac{1}{2}(\chi^2_{\rm min}+\bar{l}_i\bar{l}_jF_{ij}+\bar{p}_i\bar{p}_jP^{-1}_{ij}-\bar{d}_i\bar{d}_jD^{-1}_{ij})}\,. \tag{52}$$

As it is explained in e.g. (Amendola & Tsujikawa 2015; Amendola 2018), the evidence depends on three factors: (i) the ability of the model to fit the data of the likelihood (42). This fixes the value of $\chi^2_{\rm min}$; (ii) the relative difference between the constraints set by the likelihood and the prior. This fixes the ratio $|D|/|P|$; and (iii) the distance in parameter space between the best-fit values preferred by the likelihood and those that are preferred by the prior, which affects the computation of $\bar{l}_i\bar{l}_jF_{ij}+\bar{p}_i\bar{p}_jP^{-1}_{ij}-\bar{d}_i\bar{d}_jD^{-1}_{ij}$. The evidence automatically integrates Occam's razor criterion in its definition, since the addition of extra parameters (when we take a model with $J' > J$) reduces the value of $\mathcal{E}$ when they are constrained by the likelihood in a comparable way (or better) than by the prior. This means that the weights in our WFR method are built through (36) according to this criterion as well. On the one hand, adding more parameters reduces the value of $\chi^2_{\rm min}$ (if these parameters are effective enough, of course) and this increases the value of $\mathcal{E}$; on the other, there is the corresponding penalization, as mentioned before, so there exists a competition between these two opposite effects.

Formulas (50) and (51) are fully symmetric under the interchange of the prior and likelihood covariance matrices and best-fit values. Therefore, once we divide the data into two parts, the posterior best-fit values and associated uncertainties for a given model do not depend at all on which of these parts is used to build the prior and which is used to construct the likelihood. There is a kind of freedom at this point. It is important to remark, though, that the prior distribution cannot be built with data that already take part of the likelihood, since this would produce an unwanted double counting which would make the analysis inconsistent.

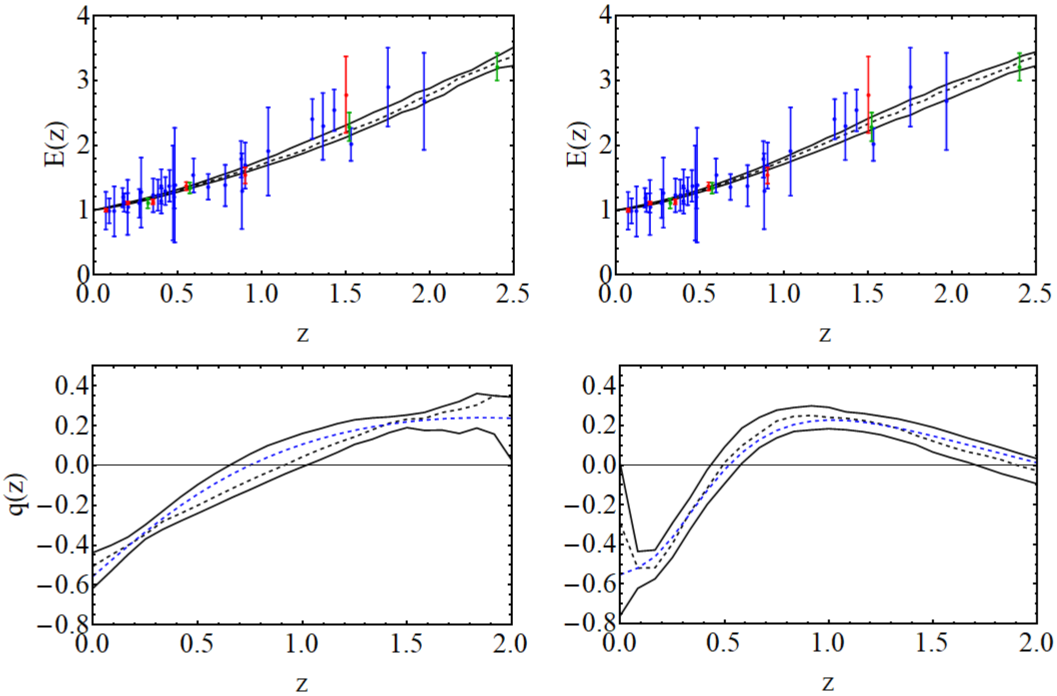

Figure 3. As in Fig. 2, but incorporating the BAOs data to the likelihood. They are depicted in green in the upper plots.

For example, we are not allowed to use the data from the JLA SnIa compilation as a prior and the Pantheon ones for the likelihood, just because the latter contains the former (cf. Sect. 2.1), and we would obtain biased constraints on the parameters of the model under study. Conversely, the evidence (52) is not symmetric under the aforementioned interchange, so the weights used in the WFR method are sensitive to it. We will analyze its impact in Sect. 4.

We can use (50) and (51) together with a multivariate Gaussian random number generator using e.g. *Mathematica*, in order to produce a list of vectors $\vec{c}$ following the posterior distribution (49). For each of these vectors we can compute the functions of interest, $E_J(z)$, $q_J(z)$, and $j_J(z)$. Notice that we do not need to carry out any Monte Carlo algorithm to do that. Thanks to the fact of having the analytical expressions (50) and (51) we can generate histograms of the aforementioned functions at the wanted redshifts without loosing the computational time that we would have to expend with a Monte Carlo exploration of the parameter space. In this way we can obtain the same level of statistics roughly three times faster, because we do not have to throw away the $\sim 60\% - 70\%$ of the points, as it is done in a typical Markov chain Monte Carlo run. We remark that the analytical obtention of (50) and (51) has been possible because the data is Gaussian-distributed (cf. Sect. 2) and also because the fitting functions (29) are linear in the coefficients c_i. The analytical computation of the evidence with formula (52) also allows us to save valuable computational time, since we can avoid the calculation of the corresponding integral in the J-dimensional parameter space, cf. the formula (36). Once we obtain the histograms with the values of the various functions evaluated at several redshifts for all the models, we can construct the corresponding join distribution (as a histogram, of course) for each function and redshift according to (38), and finally derive their WFR-reconstructed shape. We present our results in the next section.

4 RESULTS AND DISCUSSION

We start analyzing and discussing the results that we obtain applying the methodology explained in the previous section to the direct reconstruction of the Hubble rate and the derived deceleration parameter. In Fig. 2 we show the results for the case in which we use the Pantheon+MCT and CCH data, being the former employed to build the prior, and the latter to construct the likelihood (later on we will analyze the impact of this choice in detail). In the left column of this figure we present the results obtained with the WFR method when use is made of the expansion in the redshift (13), whereas those of the right column are obtained using (14), which is built in the y-variable. It is obvious that the reconstructed Hubble rates are in both cases very similar, not only concerning the central values, but also the 1σ-bands. In contrast, although the reconstructed shapes for $q(z)$ are completely compatible, one can appreciate important differences concerning the size of the error bands in some regions of the covered redshift range. This is palpable around $z = 0$. Using (13) we obtain $q_0 = -0.55^{+0.09}_{-0.11}$, whereas using (14) $q_0 = -0.54^{+0.47}_{-0.83}$ (both at 1σ c.l.), so the latter is compatible with 0 at only $\sim 1\sigma$. This is clearly pointing out some kind of defect affecting (at least) one of the two expansions. We are using the WFR method precisely to remove the model and parametrization-dependence that is inherent to many other analyses in the literature, but concerning the shape of $q(z)$ we see that this parametrization-dependence still persists, we have not been able to get rid of it. Notice more-

J	$q_{0,J}$	$z_{t,J}$	$j_{0,J}$	$\mathcal{E}_J$	$\mathrm{w}_i \equiv \frac{\mathcal{E}_J}{\sum_i \mathcal{E}_i}$
2	$-0.50^{+0.05}_{-0.04}$	$0.91^{+0.09}_{-0.06}$	$0.59^{+0.13}_{-0.12}$	318.57	0.52
3	$-0.64^{+0.09}_{-0.07}$	$0.58^{+0.17}_{-0.07}$	$1.48^{+0.25}_{-0.51}$	274.48	0.45
4	$-0.62^{+0.12}_{-0.17}$	$0.60^{+0.15}_{-0.13}$	$1.5^{+1.3}_{-1.0}$	19.74	0.03

Table 5. Current values of the deceleration and jerk parameters, transition redshift, evidence and corresponding weight for each model involved in the same WFR-reconstructions of the left column in Fig. 3, those that make use of (13). The model containing only the linear term in z, i.e. with $J = 1$, and all the models with $J > 4$ do not contribute significantly to the final reconstruction because they have a negligible weight in the global distribution (38). We have not included their information in this table. The effective number of degrees of freedom is $N_{\rm eff} = 2.52$, and the final reconstruction leads to: $q_0 = -0.51^{+0.08}_{-0.10}$, $z_t = 0.90^{+0.12}_{-0.25}$, and $j_0 = 0.59^{+0.64}_{-0.12}$.

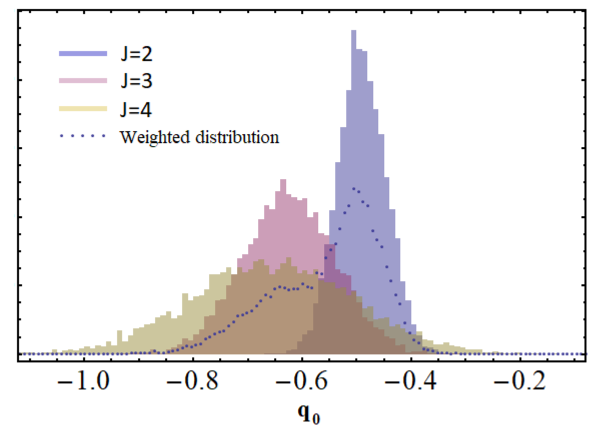

Figure 4. Individual distributions for q_0 for the various models that contribute non-negligibly to the final WFR-reconstructions of Fig. 3 (left column), cf. also Table 5. We also plot the weighted distribution, which is built from the individual ones analogously to (38).

over that the ΛCDM curves (which are drawn in green in all the plots of Fig. 2) are in all cases fully compatible at $< 1\sigma$ with the reconstructed functions. They are actually contained inside the reconstructed bands. The only exception is at a small region at $z > 1.2$ of the lower right plot, which is compatible not at one, but at two sigmas. The 1σ-bands, though, are much smaller in the ΛCDM than in the WFR-reconstructions. This is the price we have to pay for the model-independence of our analysis (which, as already said, seems not to be yet parametrizarion-independent, see the subsequent comments below).

In Fig. 3 we show the results that we obtain by also considering the BAOs information. The problem mentioned above does not disappear neither in this case. The reconstructed functions $E(z)$ are now even more resonant than before, and the error bands decrease for the Hubble rate and $q(z)$, as expected, but the reconstructed deceleration parameter still suffers from the same problems mentioned before. Now, $q_0 = -0.51^{+0.08}_{-0.10}$ with (13), and with (14) it is still compatible with 0 at 1σ. The reason of such discrepancy is not difficult to understand from a mathematical point of view. In order to ease the explanation we restrict ourselves to the case in which we truncate the series (13) and (14) at second order, yielding

$$E_z(z)-1 = az+bz^2 \quad ; \quad E_y(z)-1 = \tilde{a}\frac{z}{1+z}+\tilde{b}\left(\frac{z}{1+z}\right)^2, \tag{53}$$

respectively. The point is the following. The data at $z > 1$ have a greater impact on the coefficient $\tilde{a}$ rather than on a, just because the relative weight of the squared term in $E_y(z)$ (the one containing $\tilde{b}$) is much lower than the one in $E_z(z)$ and, therefore, the influence of those data points at higher redshifts on the first terms of the right-hand side of the expansions (53) is much bigger in $E_y(z)$ than in $E_z(z)$. For instance, at $z = 2$ we have $E_z(2) - 1 = 2(a + 2b)$ and $E_y(2) = 2(3\tilde{a} + 2\tilde{b})/9$, so the relative weight of $\tilde{a}$ is three times larger than the one of a at this redshift. By comparing (13) and (14) with (53) one can see that the relation between q_0 and the a's are exactly the same, i.e. $q_0 = a - 1$ and $q_0 = \tilde{a} - 1$, respectively, so q_0 will depend more strongly on the data points at high redshifts in the parametrization (14) than in (13). In fact, notice that if we had data points at very high redshifts, let us say at $z \to \infty$, then these data would not influence a at all, whereas $\tilde{a}$ would have the same weight as $\tilde{b}$. This situation is clearly anomalous and is probably telling us that the parametrization (14) is quite unpractical and unable to grasp properly the correct physical behavior of the underlying function, i.e. the function we aim to reconstruct, just because q_0 is too sensitive to the data at very high redshifts. We must be more confident on the constraints for q_0 obtained through (13) than the ones obtained through (14). Actually, it is quite abnormal not to find any evidence for the current accelerated phase of the Universe with (14). Conversely, with the parametrization (13) we find very strong evidence applying a full Bayesian approach. We can repeat the same procedure used to reconstruct $E(z)$, but fixing $q_0 = 0$. We compute then the sums of the evidences derived from all the models $E_J(z)$ when $q_0 = 0$, i.e. $\mathcal{E}_J(q_0 = 0)$, and when $q_0 \neq 0$ and left free in the fitting analyses, i.e. $\mathcal{E}_J(q_0 \neq 0)$. Then we calculate the Bayes ratio using these sums, as follows,

$$B = \frac{\sum_J \mathcal{E}_J(q_0 \neq 0)}{\sum_J \mathcal{E}_J(q_0 = 0)} = 1137 \to \ln B = 7.04\,. \tag{54}$$

According to Jeffreys' scale (see e.g. the references by Amendola & Tsujikawa (2015) and Amendola (2018); and also the one by Jeffreys (1961)), this is pointing towards a very strong evidence in favor of an accelerated Universe, since $\ln B > 5$[5]. Here the BAOs data play a crucial role to enhance the confidence level of our result. We have checked that if we remove them from our data set $\ln B = 2.83$ and, hence, the evidence decreases up to a moderate level, just because in this case $1 < \ln B < 3$. This in stark contrast

[5] Using the value of H_0 provided by Riess et al. (2018a) –instead of $H_0 = (70\pm5)$ km s^{-1}Mpc^{-1}– in the prior employed to convert the original CCH+BAOs data into data on the Hubble rate (see Sect. 2.2), we find $q_0 = -0.52^{+0.05}_{-0.09}$ and $\ln B = 7.96$. Using the one derived from the fitting analysis of the ΛCDM carried out by the Planck Collaboration VI (2018) with the TT+lowE CMB data we obtain $q_0 = -0.46^{+0.06}_{-0.15}$ and $\ln B = 6.07$. In both cases the strong level of evidence is maintained, so our conclusion does not depend on this.

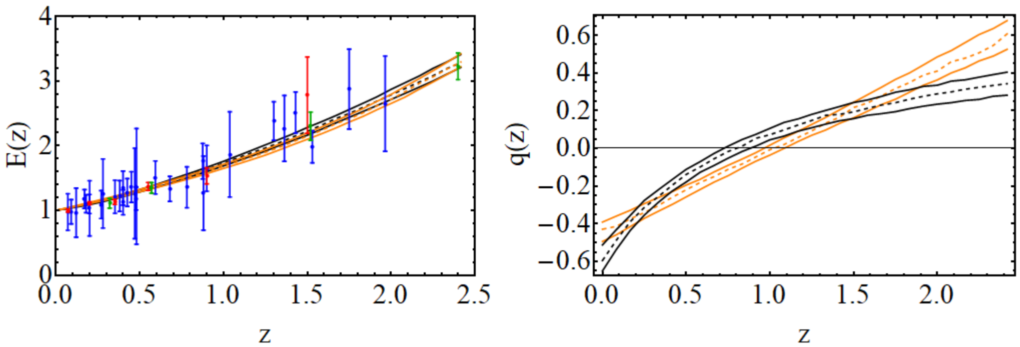

Figure 5. *Left plot:* Reconstructed Hubble rates and 1σ-bands obtained with the WFR method, using the CCH+BAO (prior) and Pantheon+MCT (likelihood) data, and the parametrizations (15, in orange) and (16, in black). The data points are depicted with the same colors of Fig. 3; *Right plot:* The corresponding reconstructed deceleration parameters.

Prior	Likelihood	q_0	z_t
SnIa	CCH	$-0.62^{+0.13}_{-0.11}$	$0.71^{+0.24}_{-0.14}$
SnIa	CCH+BAOs	-0.60 ± 0.10	$0.80^{+0.09}_{-0.12}$
CCH	SnIa	$-0.62^{+0.11}_{-0.10}$	$0.74^{+0.21}_{-0.17}$
CCH+BAOs	SnIa	$-0.60^{+0.08}_{-0.06}$	$0.81^{+0.08}_{-0.09}$

Table 6. Values of q_0 and z_t obtained from the reconstruction of $q(z)$ using the WFR and the expansion (16). We provide the results for four alternative combinations of the prior and the likelihood distributions, see related comments in the main text.

with the results found e.g. in the context of the ΛCDM (cf. Table 3), in which one founds $q_0 = -0.554 \pm 0.032$ using only the SnIa and the CCH data. These 17σ of evidence are very far away from the more conservative one that we have inferred from our model-independent approach, which has an uncertainty roughly three times bigger.

In Table 5 we provide some relevant information about the individual models (13) employed in the WFR-reconstructions of $E(z)$ and $q(z)$ that we have plotted in the left column of Fig. 3. Actually, only three of these models play an important role in these reconstructions: the third, fourth and fifth-order polynomials of $E(z)$. The other ones are strongly suppressed either because they are completely unable to fit correctly the data, as the linear expansion of $E(z)$, with $J = 1$, or because they receive a very important penalization for using too many parameters. It is the case of those models with $J > 4$. Remarkably, the central values of the parameters q_0, j_0, and also z_t, obtained with the global WFR-distribution (38) are very close to those obtained in the model with highest evidence, i.e. the one with $J = 2$. Although the addition of the other models (basically those with $J = 3, 4$) in the weighted sum only shifts very slightly the central values of the parameters, they increase the total uncertainty (compare the values in Table 5 with those provided in its caption). In order to better visualize the interplay of the various models in the generation of the final output we have also included Fig. 4. There we show the Gaussian shape of the individual distributions for q_0 obtained in the models with $J = 2, 3, 4$, together with the weighted distribution built analogously to (38). The latter departs considerably from Gaussianity.

Alternatively, we have also explored what happens if we use the expansions (15) and (16) of $q(z)$ instead of the expansions of $E(z)$ analyzed up to now. First of all we want to remark that if we use these expansions of $q(z)$ the theoretical expressions of the corresponding Hubble rates that enter the fitting analysis loose their linearity in the coefficients. Thus, we cannot obtain the exact analytical expressions for the posterior best-fit values and covariance matrix of the parameters that are used to build $q(z)$. Nevertheless, we can work with the Fisher approximations of the likelihood and posterior distributions (see e.g. Amendola & Tsujikawa (2015) and Amendola (2018)) and apply the methodology developed in the last section in order to carry out the reconstructions. In Fig. 5 we plot the reconstructed Hubble rates and deceleration parameters obtained with the WFR method and the expansions (15) and (16). The theoretical expressions for the Hubble rate are easy to compute using (10). For example, introducing (16) in (10) and integrating the resulting equation we obtain

$$E_J(z) = (1+z)^{1+\sum\limits_{i=0}^{J} q_i} e^{-\sum\limits_{k=1}^{J} \frac{1}{k}\left(\frac{z}{1+z}\right)^k \sum\limits_{i=k}^{J} q_i} \qquad (55)$$

for $J > 0$, and $E(z) = (1+z)^{1+q_0}$ for $J = 0$. Analogous expressions can be derived when we use the expansion (15). To obtain Fig. 5 we have employed the data on CCH+BAOs to build the prior and the Pantheon+MCT data for the likelihood. The left plot shows, again, that the reconstructed Hubble rates obtained from the two expansions under study, (15) and (16), are fully consistent. Moreover, the reconstructed $q(z)$'s are compatible at the $\sim 1-2\sigma$ c.l. in all the redshift range and the error bands also have a similar size. In this case the current values of the deceleration parameter read $q_0 = -0.43^{+0.04}_{-0.07}$ and $q_0 = -0.60^{+0.08}_{-0.06}$ for the parametrization (15) and (16), respectively.

We have also studied the differences that are found in the reconstruction of $q(z)$ in the context of the parametrization (16) when one uses the SnIa data in the prior and the CCH/CCH+BAOs in the likelihood instead of using the latter in the prior and the former in the likelihood. The results are shown in Fig. 6. It is evident that this particular choice only has a very minimal impact on our results, the differences are almost imperceptible at naked eye. This can be also checked in Table 6, where we list the values of q_0 and the deceleration-acceleration transition redshift z_t that are obtained for the four situations explored in Fig. 6. The latter has been proposed in the literature as a potential primary cosmological parameter, see e.g. (Lima et al. 2012).

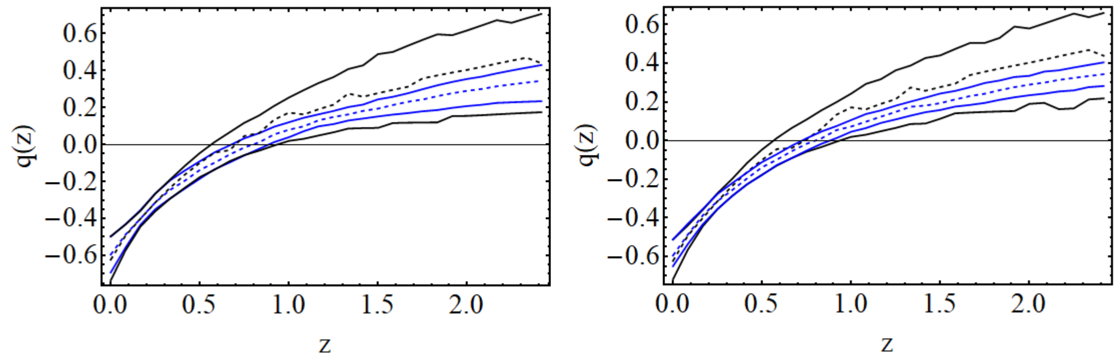

Figure 6. *Left plot:* Reconstructed deceleration parameters and 1σ-bands obtained with the WFR method and the parametrization (16). The black curves are obtained using the SnIa data in the prior and the CCH in the likelihood. The blue curves by also adding the BAOs data in the likelihood; *Right plot:* The same as in the left plot, but using the CCH and CCH+BAOs data in the prior (in black and blue, respectively), and in both cases the SnIa data in the likelihood.

The constraints are very similar as those obtained with the parametrization (13), and also as those reported in the interesting work (Haridasu et al. 2018). These authors obtained $q_0 = -0.52 \pm 0.06$ and $z_t = 0.64^{+0.12}_{-0.09}$ using the so-called Multi-Task Gaussian Processes technique and a very similar data set as the one employed by us in our analyses, considering the SnIa data of the Pantheon+MCT compilation, CCH and BAOs, as we do. The only differences are the following: they used the BAOs data from (Alam et al. 2017; Zhao et al. 2018) instead of the data provided in (Gil-Marín et al. 2017; Gil-Marín et al. 2018); and the CCH data that we have listed in the second column of our Table 2, instead of those listed in the third column of the same table, which also incorporate the systematic errors due to the choice of SPS model and those introduced by the potential presence of a young stellar component in the quiescent galaxies. The reconstructed shape of the deceleration parameter provided in their Fig. 5 is also very similar to those that we have obtained using (13) and (16) in the context of the WFR method, cf. Figs. 3 and 6, and the aforementioned figure in (Haridasu et al. 2018). Thus, there is a very good resonance between the two reconstruction techniques when a reasonable basis for the truncated series is employed in the WFR method.

We have also reconstructed the jerk parameter $j(z)$ using the expansions (13) and (15). The results are presented in Fig. 7. They are fully compatible, but unfortunately the errors are still quite large. Nevertheless we can see that the string of data on SnIa+CCH+BAOs employed in this work does not prefer any important deviation from $j(z) = 1$, i.e. the predicted value in the ΛCDM, so there is no need of introducing new physics in order to explain these observations at low and intermediate redshifts. Some authors that have found important evidence in favor of the dynamical nature of the dark energy in the context of various running vacuum and DE models and parametrizations (Solà, Gómez-Valent & de Cruz Pérez 2017; Solà, de Cruz Pérez & Gómez-Valent 2018) have also stated that in order to grasp this dynamical feature one has to use the triad of data on CMB, BAOs, and large-scale structure (especially, those data on redshift space distortions), and that the current data on SnIa and CCH do not require (when used alone) the need of new physics in the form of dynamical DE. This in perfect consonance with the results extracted from the reconstructions carried out in this work.

Finally, it is also interesting to compare our model-independent results, e.g. those compiled in Table 6, with those predicted in the ΛCDM, using the best-fit parameter of $\Omega_m^{(0)}$ obtained from the TT,TE,EE+lowE+lensing+BAO fitting analysis reported by the Planck Collaboration VI (2018), $\Omega_m^{(0)} = 0.3111 \pm 0.0056$. Using formula (21) (and setting $w_0 = -1$) one obtains $q_0 = -0.534 \pm 0.008$, and using the ΛCDM formula for the deceleration-acceleration transition redshift,

$$z_t = \left(\frac{2(1-\Omega_m^{(0)})}{\Omega_m^{(0)}}\right)^{1/3} - 1\,, \tag{56}$$

one gets $z_t = 0.64 \pm 0.01$. These values are compatible at $1-2\sigma$ c.l. with those presented in Table 6.

5 CONCLUSIONS

We have reconstructed in this paper the deceleration and jerk parameters from a very updated data set on SnIa, CCH and BAOs, using the weighted function regression method, and by only assuming the Cosmological Principle and the flatness of the Universe. We have not taken more assumptions for granted, so our analysis can be considered quite model-independent. We have corrected the CCH data in order to incorporate the effect of some systematic uncertainties that are usually disregarded in many other analyses in the literature. We have shown with concrete examples in Sect. 3.2 that if we want to infer objective constraints on the cosmographical functions we are forced not to base our fitting analyses on concrete cosmological models, specific parametrizations of the cosmographical quantities or individual truncated cosmographical expansions. We have studied the correspondance between the latter two scenarios and particular dark energy models in standard GR. The results that we have obtained from our reconstructions are consistent with the standard cosmological model, but the statistical uncertainties associated to the reconstructed functions are much larger (a factor ~ 3) than those that are obtained in the context of the ΛCDM and other particular frameworks. This is actually something expected, and is

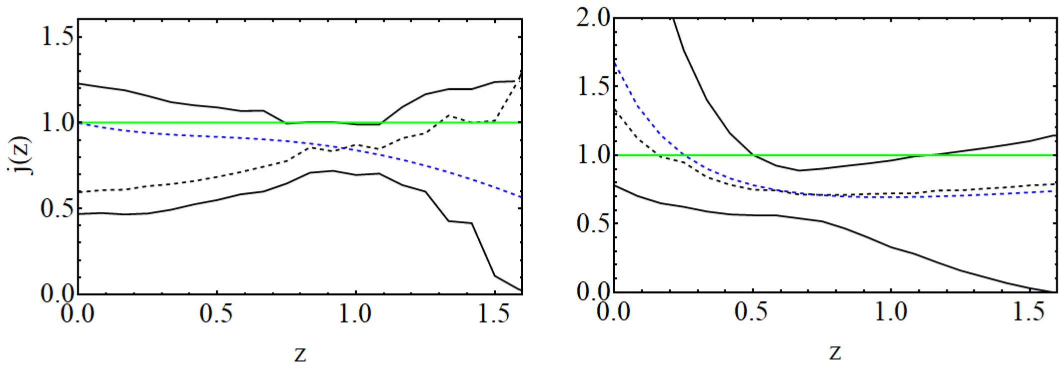

Figure 7. *Left plot:* Reconstruction of the jerk obtained in the same framework of Fig. 3, using the parametrization for $E(z)$ (14). The error bands cover the 2σ-range. We also plot the ΛCDM prediction, i.e. $j(z) = 1$, in green, and the mean of the reconstructed jerk in blue; *Right plot:* The same, but using the parametrization for $q(z)$ (16).

the price one has to pay for the model-independence. We have computed the level of evidence in favor of the current speed-up of the Universe following a full (and exact) Bayesian approach, using the tools provided in Sect. 3. We have obtained values of q_0 which lie $5-6\sigma$ away from 0 when only the SnIa of the Pantheon+MCT compilation and the CCH are considered. This is in strong contrast with the 17σ found in the concordance model using the same data. Computing the exact Bayesian evidences and using Jeffreys' scale, we have checked that this corresponds to a moderate level of evidence, whereas it is promoted to a very strong one if also the data on BAOs are taken into account. Thus, these results support the general accepted idea that the Universe is currently undergoing a positive accelerated expansion. This seems to be now something beyond doubt in the light of only low and intermediate-redshift data. Nevertheles, we want to highlight here the importance of carrying out model-independent analyses (when possible) as the one we have reported in this paper to infer unbiased information about the Cosmos, specially when substantial evidence is obtained in the context of concrete cosmological models. We could ask ourselves, for instance, what was the real evidence found by Riess et al. (1998) and Perlmutter et al. (1999) in favor of an accelerated Universe in the time these seminal papers appeared. Most probably, the 3σ c.l. evidence reported in these works would have been considerably degraded if a more model-independent method would have been applied to extract the value of q_0. This certainly is a more conservative way to proceed. Interestingly, we have also seen that our model-independent results are fully compatible with those reported by Haridasu et al. (2018), which were obtained using a generalization of the usual Gaussian Processes technique that allowed them to deal with the SnIa+CCH+BAOs data sets in the same analysis simultaneously. In addition, we have provided a new model-independent determination of the deceleration-acceleration transition redshift, $z_t \sim 0.8 \pm 0.1$, and have checked that with the low and intermediate data sets under consideration the jerk parameter does not require any deviation from the ΛCDM in order to be explained, although of course, departures from the latter (as e.g. those coming from some sort of dynamical dark energy) are still allowed given the current size of the uncertainties found for this parameter.

Nowadays, in the era of precision cosmology we are living, we know that *not* all the observational cosmology is the search for two numbers, H_0 and q_0, although these parameters certainly are the ones that can be measured in a model-independent way with better accuracy, as we have shown in this work. Here we have focused our attention on the second. The measured current value of the deceleration parameter clearly tells us that the Universe is speeding up. The causes of this positive acceleration are still unknown. We think that, in the future, cosmographical analyses as the one carried out in this paper might play an important role to decipher the mystery of the physics behind the current accelerated phase. Despite the jerk parameter is still quite unconstrained by the low and intermediate-redshift data analyzed here, we certainly hope to be capable of putting stringer limits on its value in the coming years, when we have access to more and better data thanks to e.g. the Euclid satellite or the Dark Energy Spectroscopic Instrument (DESI). This research line could provide us of new hints about the mechanism that is triggering the current speed-up of the Universe, allowing also the jerk parameter to be a good discriminator of cosmological models, and helping in this way to move towards the solution of one of the most profound enigmas in Physics.

ACKNOWLEDGMENTS

The author wants to express his gratitude to the Institute of Theoretical Physics of the Ruprecht-Karls University of Heidelberg for the financial support and hospitality during his second short postdoctoral stay there, when the idea of this work came up, and especially to Prof. Luca Amendola for his invitation and the inspiring discussions on the Bayesian evidence held during that time. The author is also grateful to Prof. Joan Solà Peracaula for reading this manuscript and for his useful comments on it.

REFERENCES

Abbott B.P., Abbott R., Abbott T.D. et al., 2017, Natur, 551, 85
Addison G.E., Watts D.J., Bennett C.L. et al., 2018, ApJ, 853, 119

Akaike H., 1974, ITAC, 19, 716
Akarsu Ö, Dereli T., Kumar S., Xu L., 2014, EPJP, 129, 22
Alam S., Ata M., Bailey S. et al., 2017, MNRAS, 470, 2617
Amendola L., 2018, Lecture notes on Statistical Methods, University of Heidelberg
Amendola L., Tsujikawa S., 2015, Dark Energy. Theory and Observations. Cambridge Univ. Press, Cambridge
Betoule M., Kessler R., Guy J. et al., 2014, A&A, 568, A22
Birrer S., Treu T., Rusu C.E. et al., 2018, arXiv:1809.01274
Blandford R.D., Amin M., Baltz E.A. et al., 2005, ASP Conf. Ser., 339, 27
Bonvin V., Courbin F., Suyu S.H. et al., 2017, MNRAS, 465, 4914
Bruzual G., Charlot S., 2003, MNRAS, 344, 1000
Camarena D., Marra V., 2018, PhRvD, 98, 023537
Cardona W., Kunz M., Pettorino V., 2017, JCAP, 1703, 056
Cattoën C., Visser M., 2007a, arXiv:gr-qc/0703122
Cattoën C., Visser M., 2007b, CQGra, 24, 5985
Chevallier M., Polarski, D., 2001, IJMPD, 10, 213
Cunha J.V., 2009, PhRvD, 79, 047301
Cunha J.V., Lima J.A.S., 2008, MNRAS, 390, 210
Dado S., Dar A., 2018, arXiv:1808.08912
Dunsby P.K.S., Luongo O., 2016, IJGMM, 13, 1630002
Dutta K., Ruchika, Roy A., Sen A.A., Sheikh-Jabbari M.M., 2018, arXiv:1808.06623
Elgarøy Ø., Multamäki T., 2006, JCAP, 0609, 002
Feeney S.M., Peiris H.V., Williamson A.R. et al., 2018, arXiv:1802.03404
Follin B., Knox L., 2018, MNRAS, 477, 4534
Gil-Marín H., Guy J., Zarrouk P. et al., 2018, MNRAS, 477, 1604
Gil-Marín H., Percival W.J., Verde L. et al., 2017, MNRAS, 465, 1757
Giostri R., Vargas dos Santos M., Waga I. et al., 2012, JCAP, 1203, 027
Gómez-Valent A., Amendola L., 2018, JCAP, 1804, 051
Gong Y-G., Wang A., 2007, PhRvD, 75, 043520
Guidorzi C., Margutti R., Brout D. et al., 2017, ApJ, 851, L36
Guimarães A.C.C., Cunha J.V., Lima J.A.S., 2009, JCAP, 0910, 010
Guimarães A.C.C., Lima J.A.S., 2011, CQGra, 28, 125026
Haridasu B.S., Luković V.V., D'Agostino R., Vittorio N., 2017, A&A, 600, L1
Haridasu B.S., Luković V.V., Moresco M., Vittorio N., 2018, arXiv:1805.03595
Hastings W., 1970, Biometrika, 57, 97
Heneka C., 2018, arXiv:1809.04043
Hotokezaka K., Nakar E., Gottlieb O. et al., 2018, arXiv:1806.10596
Ishida E.E.O., Reis R.R.R., Toribio A.V., Waga I., 2008, ApJ, 28, 547
Jang I.S., Lee M.G., 2017, ApJ, 836, 74
Jeffreys H., 1961, Theory of Probability. Clarendon Press, Oxford
Jesus J.F., Holanda R.F.L., Pereira S.H., 2018, JCAP, 1805, 073
Jiménez R., Loeb A., 2002, ApJ, 573, 37
Jiménez R., Verde L., Treu T., Stern D., 2003, ApJ, 593, 622
Keenan R.C., Barger A.J., Cowie L.L., 2013, ApJ, 775, 62
Knop R.A., Aldering G., Amanullah R. et al., 2003, ApJ, 598, 102
Lemos P., Lee E., Efstathiou G., Gratton S., 2018, arXiv:1806.06781
Lima J.A.S., Jesus J.F., Santos R.C., Gill M.S.S., 2012, arXiv:1205.4688
Linder E.V., 2003, PhRvL, 90, 091301
Linder E.V., 2004, PhRvD, 70, 023511
López-Corredoira M., Vazdekis A., 2018, A&A, 614, A127
López-Corredoira M., Vazdekis A., Gutiérrez C.M., Castro-Rodríguez N., 2017, A&A, 600, A91
Lu J., Xu L., Liu M., 2011, PhLB, 699, 246
Luongo, O. 2011, MPLA, 26, 1459
Mamon A.A., 2018, MPLA, 33, 1850056
Mamon A.A., Bamba K., 2018, arXiv:1805.02854
Mamon A.A., Das S., 2017, EPJC, 77, 495
Maraston C., Strömbäck G., 2011, MNRAS, 418, 2785
Marra V., Amendola L., Sawicki I., Valkenburg W., 2013, PhRvL, 110, 241305
Mas des Bourboux H., Le Goff J-M., Blomqvist M. et al., 2017, A&A, 608, A130
Metropolis N., Rosenbluth A., Rosenbluth M., Teller A., Teller E., 1953, JChPh, 21, 1087
Moresco M., 2015, MNRAS, 450, L16
Moresco M., Cimatti A., Jiménez R. et al., 2012, JCAP, 1208, 00
Moresco M., Jiménez R., Verde L. et al., 2018, arXiv:1804.05864
Moresco M., Pozzetti L., Cimatti A. et al., 2016, JCAP, 1605, 014
Mörtsell E., Clarkson C., 2009, JCAP, 0901, 044
Mukherjee A., Banerjee N., 2016, PhRvD, 93, 043002
Nair R., Jhingan S., Jain D., 2012, JCAP, 1201, 018
Nesseris S., García-Bellido J., 2013, JCAP, 1308, 036
Nielsen J.T., Guffanti A., Sarkar S., 2016, NatSR, 6, 35596
Ooba J., Ratra B., Sugiyama N., 2018, ApJ, 864, 80
Perlmutter S., Aldering G., Goldhaber G. et al., 1999, ApJ, 517, 565
Pinho A.M., Casas S., Amendola L., 2018, arXiv:1805.00027
Planck Collaboration XIII, 2016, A&A, 594, A13
Planck Collaboration VI, 2018, arXiv:1807.06209
Rapetti D., Allen S.W., Amin M.A., Blandford R.D., 2007, MNRAS, 375, 1510
Ratsimbazafy A.L. et al., 2017, MNRAS, 467, 3239
Riess A.G., Casertano S., Yuan W. et al., 2018a, ApJ, 855, 136
Riess A.G., Filippenko A.V., Challis P. et al., 1998, AJ, 116, 1009
Riess A.G., Macri L.M., Casertano S. et al., 2011, ApJ, 730, 119 [Erratum ibid, 2011, ApJ, 732, 129]
Riess A.G., Macri L.M., Hoffmann S.L. et al., 2016, ApJ, 826, 56
Riess A.G., Nugent P.E., Schmidt B.P. et al., 2001, ApJ, 560, 49
Riess A.G., Rodney S.A., Scolnic D.M. et al., 2018b, ApJ, 853, 126
Riess A.G., Strolger L-G., Tonry J. et al., 2004, ApJ, 607, 665
Ringermacher H.I., Mead L.R., 2016, arXiv:1611.00999
Romano A.E., 2018, IJMPD, 27, 1850102
Rubin D., Hayden B., 2016, ApJ, 833, L30
Sandage A., 1970, PhT, 23, 34
Sahni V., Saini T.D., Starobinsky A.A., Alam U., 2003, JETPL, 77, 201; 2003, PZETF, 77, 249
Schwarz G., 1978, AnSta, 6, 461
Scolnic D.M., Jones D.O., Rest A. et al., 2018, ApJ, 859, 101
Semiz I., Çamlibel K., 2015, JCAP, 1512, 038
Shafieloo A., 2007, MNRAS, 380, 1573
Shafieloo A., 2012, JCAP, 1208, 002
Shafieloo A., Alam U., Sahni V., Starobinsky A.A., 2006, MNRAS, 366, 1081
Shapiro C., Turner S., 2006, ApJ, 649, 563
Simon J., Verde L., Jiménez R., 2005, PhRvD, 71, 123001
Solà J., de Cruz Pérez J., Gómez-Valent A., 2018, MNRAS, 478, 4357
Solà J., Gómez-Valent A., de Cruz Pérez J., 2017, ApJ, 836, 43
Stern D., Jiménez R., Verde L. et al., 2010, JCAP, 1002, 008
Turner M.S., Riess A.G., 2002, ApJ, 569, 18
Turner M.S., White M., 1997, PhRvD, 56, R4439
Tutusaus I., Lamine B., Blanchard A., 2018, arXiv:1803.06197
Tutusaus I., Lamine B., Dupays A., Blanchard A., 2017, A&A, 602, A73
Vargas dos Santos M., Reis R.R.R., Waga I., 2016, JCAP, 1602, 066
Verde L., Bellini E., Pigozzo C. et al., 2017, JCAP, 1704, 023
Visser M., 2004, CQGra, 21, 2603
Visser M., 2005, CQGra, 37, 1541
Vitagliano V., Xia J-Q., Liberati S., Viel M., 2010, JCAP, 1003, 005

Weinberg S., 1972, Gravitation and Cosmology: Principles and Applications of the General Theory of Relativity. Wiley, New York
Xu L., Li W., Lu J., 2009, JCAP, 0907, 031
Xu L., Wang Y., 2011, PhLB, 702, 114
Yu H., Ratra B., Wang F-Y., 2018, ApJ, 856, 3
Zhai Z-X., Zhang M-J., Zhang Z-S. et al., 2013, PhLB, 727, 8
Zhang B.R., Childress M.J., Davis T.M. et al., 2017, MNRAS, 471, 2254
Zhang C., Zhang H., Yuan S. et al., 2014, RAA,14, 1221
Zhao G-B., Wang Y., Saito S. et al., 2018, arXiv:1801.03043